# INERTIAL EFFECT IN ALUMINUM METAL FOAMS

**A Thesis Submitted to**
**the Graduate School of Engineering and Sciences of**
**İzmir Institute of Technology**
**in Partial Fulfillment of the Requirements for the Degree of**

**MASTER OF SCIENCE**

**in Mechanical Engineering**

**by**
**Onur KOCATÜRK**

**December 2011**
**İZMİR**

We approve the thesis of **Onur KOCATÜRK**

**Prof. Dr. Mustafa GÜDEN**
Supervisor

**Prof. Dr. Hasan YILDIZ**
Committee Member

**Assist. Prof. Dr. H. Seçil ARTEM**
Committee Member

**15 December 2011**

**Prof. Dr. Metin TANOĞLU**
Head of the Department of
Mechanical Engineering

**Prof. Dr. R. Tuğrul SENGER**
Dean of the Graduate School of
Engineering and Sciences

# ACKNOWLEDGMENTS

I would like to express my sincere gratitude to my supervisor Prof. Dr. Mustafa GÜDEN for his valuable advises, great patience, guidance and encouragement through the thesis. His support and kindness are greatly appreciated. I have been fortunate to have Prof. Dr. GÜDEN as my advisor and I consider it an honor working with him.

Furthermore, I wish to thank my family who deserve a special mention for their endless support and prayers. My father, İrfan KOCATÜRK, is the person who helped and directed me during my whole education life to be successful. My mother, Havva KOCATÜRK, is the one who sincerely raised me with her caring and gently love. My brother Orkun KOCATÜRK thanks for his supports. I would like to thank also my girlfriend H. Özge BİLİR whose love, patience and permanent confidence in me, has made the life easier during my study.

Finally, I would like to thank all of my lab-mates who especially played great role in my experimental, numerical analysis and writing studies for their precious efforts.

# ABSTRACT


## INERTIAL EFFECT IN ALUMINUM METAL FOAMS

In this study, Al tubes, Al foams of different types, Al sandwich plates of various configurations (orientations) and brittle glass foam samples were quasi-statically reloaded in order to assess any micro inertia effect on the deformation stresses. Al foams tested quasi-statically were further reloaded (interrupted test) in Split Hopkinson Bar (SHPB) at dynamic strain rates in order to see effect of strain rate on micro inertia effect. Al empty tubes experienced micro inertia independent (Type I) deformation behavior in lateral compression and micro inertia dependent (Type II) deformation behavior in axial compression. The lack of strain rate sensitivity of the tested Alulight (AlSi10) closed cell Al foams (Al/Si) produced through powder route within the studied strain rate regime was attributed to the foam cell wall fracture during cell wall buckling. While Al foams with and without SiC addition showed micro inertia effect through progressive cell wall bending. In accord with these observations, Al and Al/SiC foams showed the strain rate sensitive, while Alulight foams showed strain rate insensitive plateau stress in the SHPB compression tests. The layer configuration/orientation was shown to affect Al sandwich plate deformation. Progressive bending of the interlayer fins resulted in strain rate depending crushing stress, while shearing of the interlayer resulted in strain rate insensitive deformation stress. As was expected, the strength enhancement was not seen in glass foam specimens tested as the cell walls were fractured under compressive loads. Finally, a simple testing method was shown to investigate micro inertia effect in hollow and cellular Al structures.

# ÖZET

## ALÜMİNYUM METAL KÖPÜKLERDE ATALET ETKİSİ

Bu çalışmada Al tüp malzemeler, farklı türlerdeki Al köpükler, çeşitli konfigürasyon/oryantasyonlardaki Al sandviç plakalar ve kırılgan cam köpük malzemelere deformasyon gerilmelerine etkiyen mikro atalet etkisini incelemek üzere quasi-statik yeniden yükleme testleri uygulandı. Quasi-statik olarak test edilen ve test belli bir uzama miktarına eriştiğinde durdurulan Al köpük malzemeler, daha sonra şekil değiştirme hızının mikro atalet etkisiyle ilişkisini görmek üzere Split Hopkinson Bar (SHPB) cihazında dinamik hızlarda test edildi. Boş Al tüplerde yanal basma testlerinde mikro atalet etkisine duyarsız (Tip 1) deformasyon davranışı, eksenel basma testlerinde ise mikro atalet etkisine duyarlı (Tip2) deformasyon davranışı gözlenmiştir. Toz metalurjisi yöntemi ile üretilen kapalı hücreli Al köpük (Al/Si) olan Alulight (AlSi10) malzemenin çalışılan hızlarda, şekil değiştirme hızına duyarlılığının az oluşunun sebebi hücre duvarlarındaki bükülme esnasında hücre çeperlerinde oluşan kırılmalardır. SiC katkılı ve katkısız Al köpük malzemeler ise hücre duvarlarının kademeli bükülmesi ile mikro atalet etkisi göstermiştir. Bu gözlemler doğrultusunda, SHPB basma testlerinde SiC katkılı ve katkısız Al köpükler şekil değiştirme hızına duyarlılık gösterirken, Alulight köpükler şekil değiştirme hızına duyarsız plato gerilmesi gösterdi. Katman konfigürasyonunun/oryantasyonunun Al sandviç plakaların deformasyonunda etkili olduğu gözlenmiştir. Plakaların birbirleri üzerinde kayması sonucunda şekil değiştirme hızına duyarsız deformasyon gerilimi oluşurken, plakalar arasındaki kanatçıkların kademeli bükülmesi şekil değiştirme hızına duyarlı deformasyon gerilimi gözlememizi sağlamıştır. Basma yükleri altında hücre duvarlarında kırılmalar oluşan cam köpük malzemelerde ise beklendiği üzere mukavemet artışı gözlemlenmiştir. Sonuç olarak, boşluklu ve hücreli Al yapılardaki mikro atalet etkisini araştırmak için basit bir test yöntemi gösterildi.

# TABLE OF CONTENTS

# LIST OF FIGURES

**Figure** **Page**

# CHAPTER 1

# INTRODUCTION

Most of the engineering materials including cellular and porous light-weight materials are inspired from natural materials such as cork, wood, sponge and trabecular bone and honeycomb. Engineered cellular materials such as honeycombs and foams are made from a variety of the materials including metals, polymers, ceramics and glasses. These materials are well known with their light weight, crashworthiness, noise reduction, isolation and energy absorption properties. As the metallic cellular materials, honeycombs, foams, hollow sphere agglomerates and lattices, have been increasingly find newer applications in the energy absorbing structures including aeronautical, automotive and defense industry, the research interests have recently been focused on the impact behavior (Deshpande and Fleck 2000, Gibson 1988, Klintworth and Stronge 1988, Langseth and Hopperstad 1996, Zhao and Abdennadher 2004). Among them, Al based closed cell foams are taking considerable interests. Aluminum foams are relatively easy to produce, cheap, easy to machine and can withstand large strains at a nearly constant stress, absorbing the kinetic energy of an impact without generating high peak stresses. In the deformation energy absorption applications, Al foams are noted to be more suitable than polymeric foams, because of their high strength to weight ratio, good impact resistance and excellent energy dissipation capacity. Aluminum foams deforms plastically under impact loads with essentially no spring back, preventing further impact damage (Beals and Thompson 1997). The engineering applications of Al foams and in general the metal foams are classified in three groups: light-weight construction, energy absorption and damping insulation as depicted in Figure 1.1. In energy absorption applications, the strength and shape of the stress-strain curves of the metal foams determine the amount and efficiency of the energy absorption. In the impact loading of metal foams, the strain rates may however increase significantly over quasi-static strain rates. Therefore, the high strain rate deformation properties of metal foams are important and should be included in the designing of the structures with these materials for the applications involving impact load mitigation.

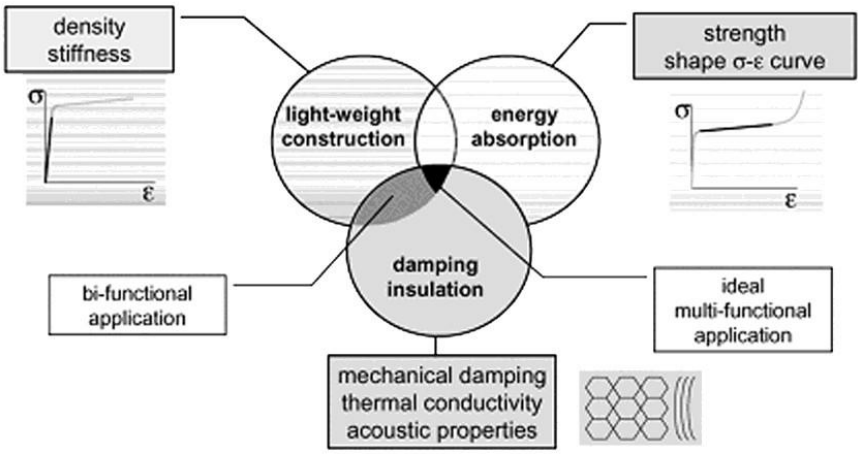


Figure 1.1. Application fields of metal foams.
(Source: Banhart 2005)

## 1.1. High Strain Rate Deformation Behavior of Cellular Materials

An out-of-plane crushing model of honeycombs under quasi-static loading was previously developed by Wierzbicki (1983), basing on the micromechanical analysis. The model developed predicted the crushing stress of the honeycombs. Later, Calladine and English (1984) showed that two effects described the dynamic behavior of energy absorbing structures: strain-rate factor and the inertia factor. The first term is referred to the material strain rate sensitivity and the second one is referred to the inertial forces at the increasing strain rates. Gibson and Ashby (1988) developed an analytical model, in which the ratio of cellular material strength over that of the cell wall material depended on a power function of the relative density. It was shown by the same investigators that the rate sensitivity of the base material determined the strain rate sensitivity of the cellular structure. Klintworth and Stronge (1988) developed constitutive equations for the large deformations of transversely crushed honeycomb materials. The cell deformation was shown to localize within the thin bands. Tam and Calladine (1991) showed that the structures, which deformed with an initial peak load followed by a falling load in the quasi-static loading, exhibited both inertia and strain-rate effects under impact loading. In the same study, a large number of tests were performed on mild steel and Al alloy. The tests results showed explicitly the effect of inertia and strain rate on the impact behavior of these materials. Goldsmith and Sackman (1992) investigated the impact behavior of honeycombs and sandwich plates. It was shown that

the mean crushing stress increased up to %50 with respect to static values in out-of-plane crushing. Reid and Peng (1997) experimentally investigated uniaxial dynamic crushing of cylindrical wood specimens. It was shown that the deformation was localized at both quasi-static and dynamic strain rates and a rate-independent simple material shock model was developed to predict the dynamic enhancement of the crushing strength of the wood. It was also reported that the collapse mode under dynamic loading of cellular structures switched from quasi-static mode to a new mode involving additional stretching which dissipated more energy. Kenny (1996) investigated the quasi-static ($1x10^{-3}$ $s^{-1)}$ and high strain rate (~$1x10^{2}s^{-1}$ ) compression behavior of an Al alloy closed cell foam (Alcan foam) with the densities of 0.31 and 0.17 g $cm^{-3}$. The lack of strain rate sensitivity in plateau stresses of Al foams tested was attributed to the brittle nature of the cells walls, allowing the gas to escape at low strains. Wu and Jiang (1997) experimentally tested six types of honeycomb structures under quasi-static and impact loads. The crush strength of the honeycombs in the axial direction showed up to 74% increase in dynamic tests. Zhao and Gary (1998) tested honeycombs in a viscoelastic Split Hopkinson Pressure Bar (SHPB) to improve the accuracy of measurement and found strain rate dependent crushing strengths of honeycomb. Lankford and Dannemann (1998) found that compressive strength of an open cell Al foam (Duocel foam) was insensitive to the applied strain rate in the range between $1x10^{-3}$ and 1200 $s^{-1}$. Mukai et al. (1999) investigated the compression behavior of Alporas closed-cell Al foam at a strain rate of $1x10^{-3}$ $s^{-1}$ and $2.5x10^{3}$ $s^{-1}$ and found that the yield stress of the Al foam exhibited 50% increase at high strain rates tests. Deshpande and Fleck (2000) tested Alulight closed-cell and Duocel open-cell foams at strain rates up to 5000 $s^{-1}$ and found that the plateau stress was almost insensitive to strain rate. Paul and Ramamurty (2000) reported that the increased plateau stresses of Alporas foam at increasingly high strain rates resulted from the micro-inertial effects. Hall et al. (2000) showed that 6061-Al alloy foam produced by powder metallurgical method (Alulight) showed no strain rate sensitivity in plateau stress with the strain rate regime of $1.5x10^{-3}$ $s^{-1}$ and 2000 $s^{-1}$. Ruan and co-workers (2003) and Zheng and co-workers (2005) showed that the plateau stress of Al honeycombs increased with the increasing the impact velocity. Ruan and co-workers (2003) further developed a model for the impact velocity dependent plateau stress. Vural and Ravichandran (2003) showed that the folding wave-length in Balsa wood became smaller under impact loading, resulting in higher crushing strength. It was also concluded that inertia effects

in progressive folding created stress enhancement even in the case of no wave-length change. Zhao et al. (2006) studied experimentally the impact behavior of Al honeycombs, Alulight and Cymat foams and hollow sphere agglomerates. The increase in the crushing strength at increasing strain rates was attributed to micro-inertia of the successive deformation. Ma et al. (2009) developed a numerical model based on Voronoi tessellation cells to determine the effect of strain rate on the crushing behavior of cellular materials. The increase of the crushing stress at the impact side under dynamic conditions was due to the inertial effect of cell walls. Fang et al. (2010) tested metallic cellular material using nylon Hopkinson bar and concluded that the strength increased at high strain rates due inertia effect. Shen and Ruan (2010) compression tested Alporas foam at the strain rates in the range of $1x10^{-3}$ to $2.2x10^{2}$ $s^{-1}$, with each test being at a fairly constant strain rate. A strain rate sensitive plateau stress was shown and the densification strain decrease with increasing strain rate.

Above studies pointed out the increase plateau stress in cellular materials particularly in Al foams and honeycombs was due to the inertia effect. It was also note that Al foams produced by different methods showed quite different responses to the increasing strain rates. Although, Alporas foam was found to show a strain rate dependent plateau stress, Alulight foam showed no strain rate sensitive plateau stress. Although strain rate sensitivity of Al foams was claimed to be resulted from micro-inertia effect, no assessment and no correlation have been made between the deformed shape of the cellular structure and the extent of micro-inertia effects. There has been also no simple method of assessing the extent of micro-inertia effect at increasing strain rates. In this thesis, the micro-inertia effects in light weight structures made of Al and Al foams with/without SiC particles and produced by different processing methods were assessed by using quasi-static reloading tests, from $1x10^{-3}$ $s^{-1}$ to $1x10^{-1}$ $s^{-1}$. The deformation of the cells was further correlated with the micro-inertia effects. The micro-inertia effects were also determined at increasingly high strain rates using SHPB, from $1x10^{-3}s^{-1}$ to 1000 $s^{-1}$. This work specifically emphasized the effect of crushing behavior of Al foams on the strain rate sensitive plateau stress behavior.

# CHAPTER 2

# AL CLOSED-CELL FOAMS: STRUCTURE, PROCESSING AND MECHANICAL BEHAVIOR

## 2.1. Foams

Foams refer to a group of cellular materials in which the gas bubbles (cells) are regularly distributed in a liquid phase. When the liquid phase is a molten metal, the foam retains its cellular structure in the solid state upon rapid solidification. The solidified cellular metal structures constitute a group of materials known as foamed metal or foam metal. Almost any metal can be foamed, while the foams of light metals such as Al and magnesium have been preferred. Foams can be presented as the interconnected network of solid struts or plates which form the edges and faces of cell as shown in Figure 2.1 (Ashby, et al. 2000). These can be classified into two groups in terms of their structures: open cell foams which are made up from only cell edges as struts and closed cell foams which are made up from both cell edges and cell faces as struts and plates, respectively. A foam structure is composed of three parts; cell face, cell edge and cell vertices as shown in Figure 2.2. Cell face is the wall between two cells, cell edge is the region where three cell walls intersect and cell vertice is the node where four cell walls intersect (Figure 2.3). Since there are only cell edges in open cell foams, the cells are connected through open faces. In closed cell foams, each cell is sealed off from its neighbors by the solid thin faces as seen in Figure 2.4.

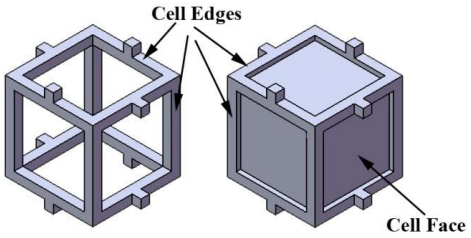


Figure 2.1. Schematic view of open and closed cell cellular structure.
(Source: Gibson and Ashby 1997)

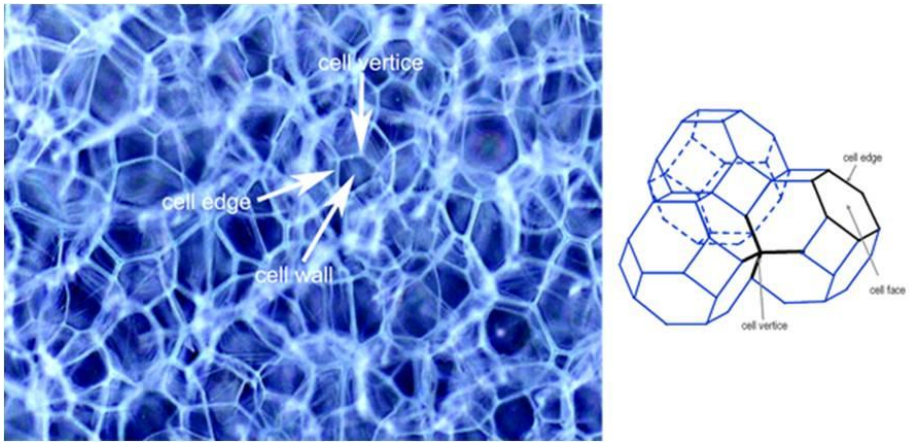


Figure 2.2. Schematic view of closed cell cellular structure.

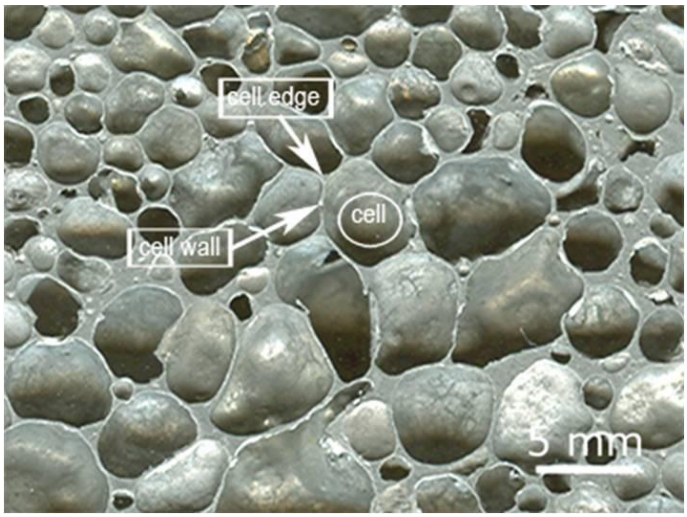


Figure 2.3. Cross-section view of a closed-cell Al foam.

## 2.2. Applications of Al Foams

Aluminum foams have the properties of low density, high stress and stiffness to weight ratio, crushing nearly at a constant load, high specific energy absorption, good acoustic and thermal insulation and recyclable. Al foams may have find applications in (i) crash energy absorption, (ii) light weight material system of composing of Al foam and (iii) sound absorption. Al foams have potentials to be used in automobiles as crash energy-absorbing filler in various places. There are two main groups of energy absorbers used in automobiles: (a) for relatively low impact energies such as bumpers and crash boxes (Figure 2.4) for frontal collision and for relatively large impact energies

such as side beams (B-pillars) to avoid severe intrusion in the passenger compartment. The foam-filled sections may also be used in the A-pillar and roof frame structures to reduce the roof crushing in roll-over accident.

Polymeric foams are known to be widely used as core material in sandwich panels. The mechanical properties of polymeric foams are however moisture dependent; therefore, their applications are limited to the ambient temperature. These disadvantages may be overcome using metal foams in sandwich panels as core materials. Aluminum foam sandwich (Figure 2.5) structures may also be used as cooling system or acoustic damper, giving multi-functional properties besides structural use. Further, the complex sandwich structure can be produced more easily with using Al foams in sandwich structures.

The sound absorption of closed-cell Al alloy foams increases with the applied rolling/compression (Güden and Kavi 2006). The rolled foam samples showed sound absorption coefficients and peak sound absorption frequencies comparable with that of glass wool as shown in Figure 2.6. The improved foam sound absorption behavior was attributed to the viscous flow across the small cracks, which resulted in passage ways for the in-and-out movement of air particles.

Figure 2.4. Impact energy absorption components for cars.

Figure 2.5. Isotropic cores for sandwich panels and shells

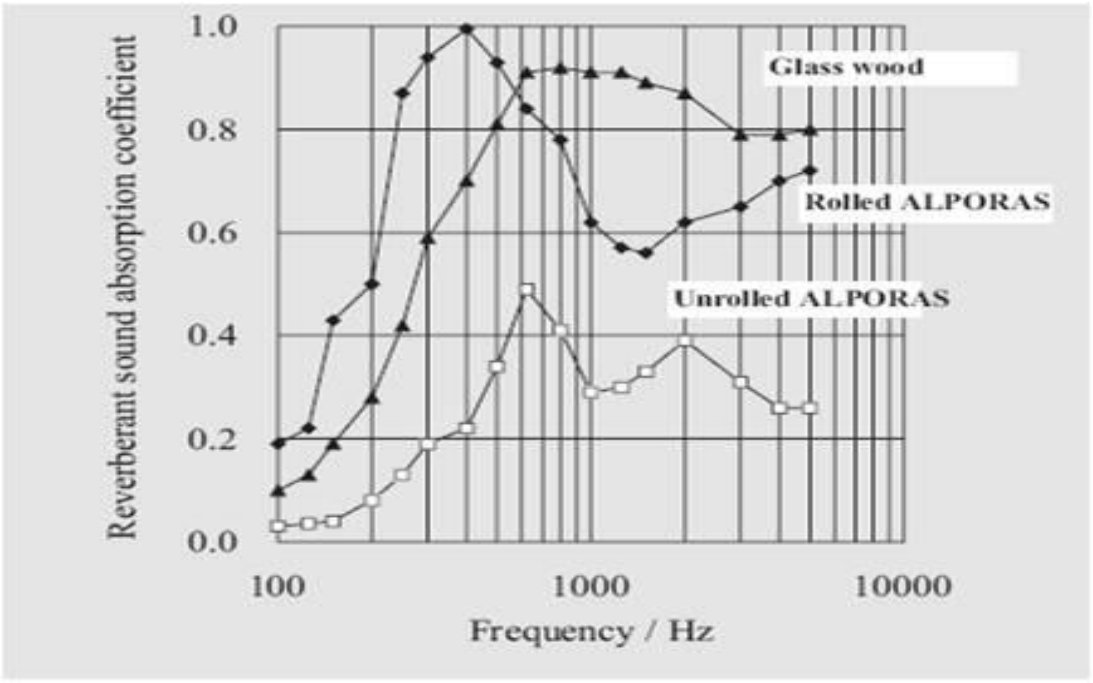


Figure 2.6. Sound absorption coefficient of Alporas foam of relative density ~0.09 (Source: Miyoshi, Itoh et al. 2000)

## 2.3. Production Methods of Closed Cell Al Foams

Al closed cell foams can be produced via foaming melts by gas injection, foaming of melts with blowing agents, foaming powder compacts process, accumulative roll-bonding technique and laser assisted foaming.

### 2.3.1. Foaming of Melts by Gas Injection

Gas injection is one of the commonly used methods of producing Al foams, Figure 2.7. Air, carbon dioxide, nitrogen or argon are injected through the foaming melt via a rotating shaft which generates fine gas bubbles and distributes them homogeneously in the melt. Particles such as Aaluminum oxide, magnesium oxide or silicon carbide are added into liquid metal in order to stabilize the gas bubbles and increase the viscosity of liquid metal.

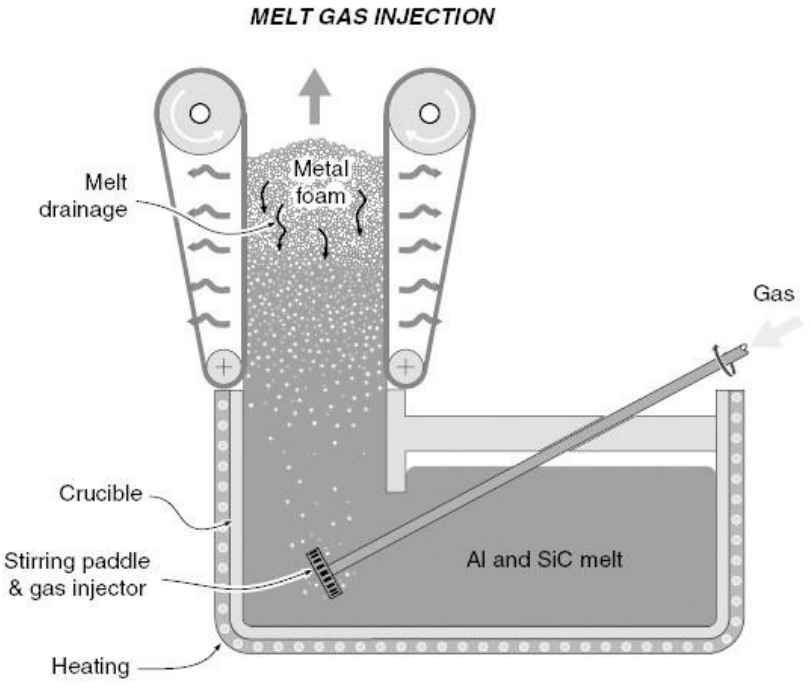


Figure 2.7. Foaming melts by gas injection.
(Source: Ashby, Evans et al. 2000)

Foaming of melts by gas injection is currently used by Alcan N. Hydro (Norway) and Cymat Aluminum Corporation (Canada). The manufacturing cost of foaming by gas injection into molten metal is relatively low; while the investment cost is high. The relative density of Al foams produced by this method ranges between 0.03 and 0.1 (Degischer 2003). The hard particles in the metal matrix; however, make these foams relatively brittle and reduce the machinability (Banhart, et al. 1996).

### 2.3.2. Foaming of Melts with Blowing Agents

In this method, the molten is foamed using a blowing agent ($TiH_2$) in order to produce Al closed cell foam (Baumgärtner, et al. 2000). Blowing agent addition process involves three steps (Kitazono, et al. 2004) as seen in Figure 2.8: (i) thickening of molten metal, (ii) adding $TiH_2$ into the molten metal and (iii) cooling the foamed liquid metal. During thickening the molten metal, 1.5% wt. calcium metal is added into the liquid Al at 680$^{o}$C and then the melt is stirred quickly. Calcium oxide, calcium-aluminum oxide or $Al_4Ca$ inter-metallic addition thickens the liquid metal and increases the viscosity (Kathuria 2001). The viscous and thickened molten metal is then poured into a casting mold while adding $TiH_2$ 1.6% wt. at 680$^{o}$C. The addition of $TiH_2$ releases the hydrogen gas in the hot viscous liquid metal as

$$TiH_2\,(s) \rightarrow Ti\,(s) + H_2(g) \qquad (2.1)$$

Upon release of hydrogen, the molten liquid metal expands in the mold and turns into liquid foam at a constant pressure. Processing of the foam such as cutting and machining is needed after cooling operation and the complicated temperature changes and difficulty in the adjustment of variables are the disadvantages of the process.

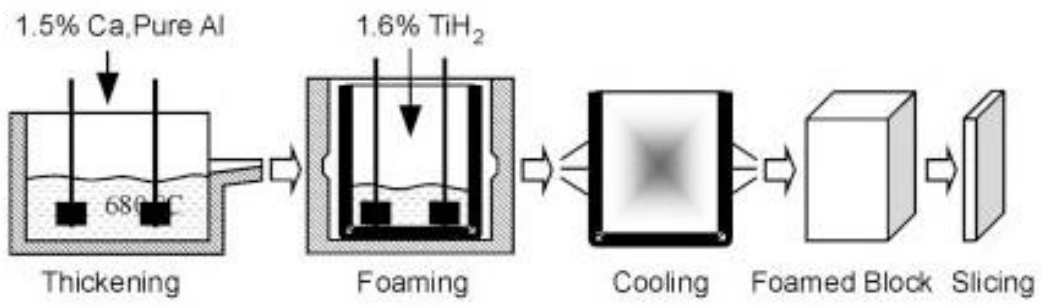


Figure 2.8. Alporas foaming technique.
(Source: Degischer 2003)

### 2.3.3. Foaming Powder Compacts Process

In this method, the Al or Al alloy powders are first mixed with foaming agent of $TiH_2$ powder (Figure 2.9). The composition is then compressed into a dense compact over 98% relative density. The cold or hot compression, extrusion and rolling can be used to form dense titanium hydride and Al powder mixture. The dense compact is heated up near to the melting point of the Al. The released gas from the blowing agent gives rise to expansion of the molten metal and the formation of the foamy structure (Guden and Yüksel 2006).

Other than metal hydrides (e.g. $TiH_2$), carbonates (e.g. calcium carbonate, potassium carbonate, sodium carbonate and sodium bicarbonate), hydrates (e.g., Al hydrate and aluminum hydroxide) or substances that evaporate quickly (e.g., mercury compounds or pulverized organic substances) can also be used as blowing agent.

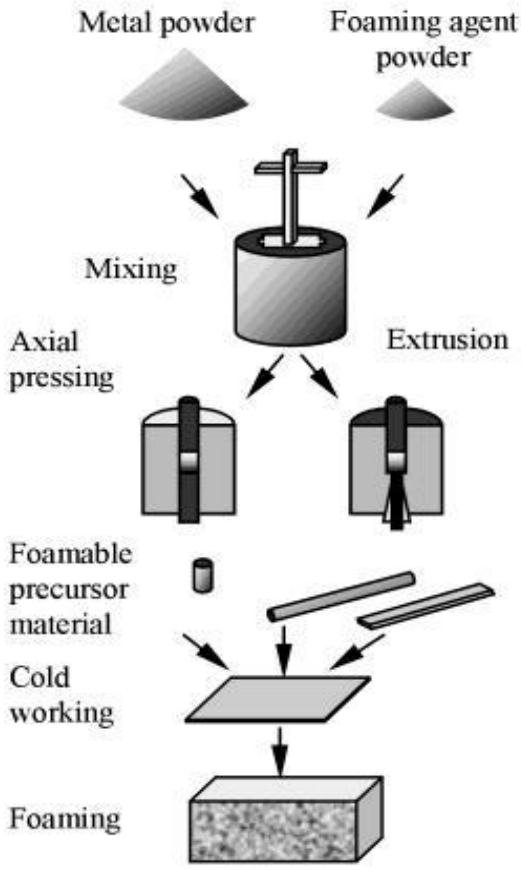


Figure 2.9. Foaming from powder compacts.
(Source: Baumgärtner, Duarte et al. 2000)

### 2.3.4. Accumulative Roll-Bonding Technique

The accumulative roll-bonding technique is the process of stacking two metal strips together with the blowing agent powder ($TiH_2$) as seen in Figure 2.10. The strips are roll-bonded by the reduction of thickness and cut into two pieces. After the surface treatment process, the pieces are stacked together again with blowing agent powder in between them and roll-bonded. Several times of roll-bonding and cutting are applied until the blowing agent particles are homogeneously dispersed in metal matrix. The rolled composite metal is then ready to foam in the following high temperature foaming process (Gibson 2000).

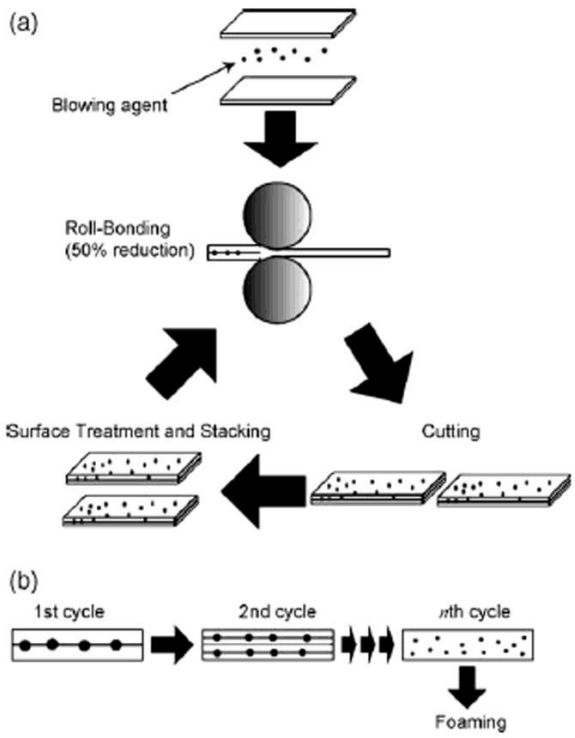


Figure 2.10. (a) Schematic of foamable precursor preparation in ARB process and (b) gradual dispersion of blowing agent particles in the rolling cycles. (Source: Kitazono, Sato et al. 2004)

### 2.3.5. Laser Assisted Foaming

Laser assisted foaming process is almost nearly the same process with the foaming powder compacts process except for heating up the compact to the melting point is done by high power laser beam irradiation as shown in Figure 2.11 (Gibson 2000). The expansion of the dense compact during foaming operation is local and unidirectional in the direction of laser irradiation. The expansion in the other directions is relatively negligibly small.

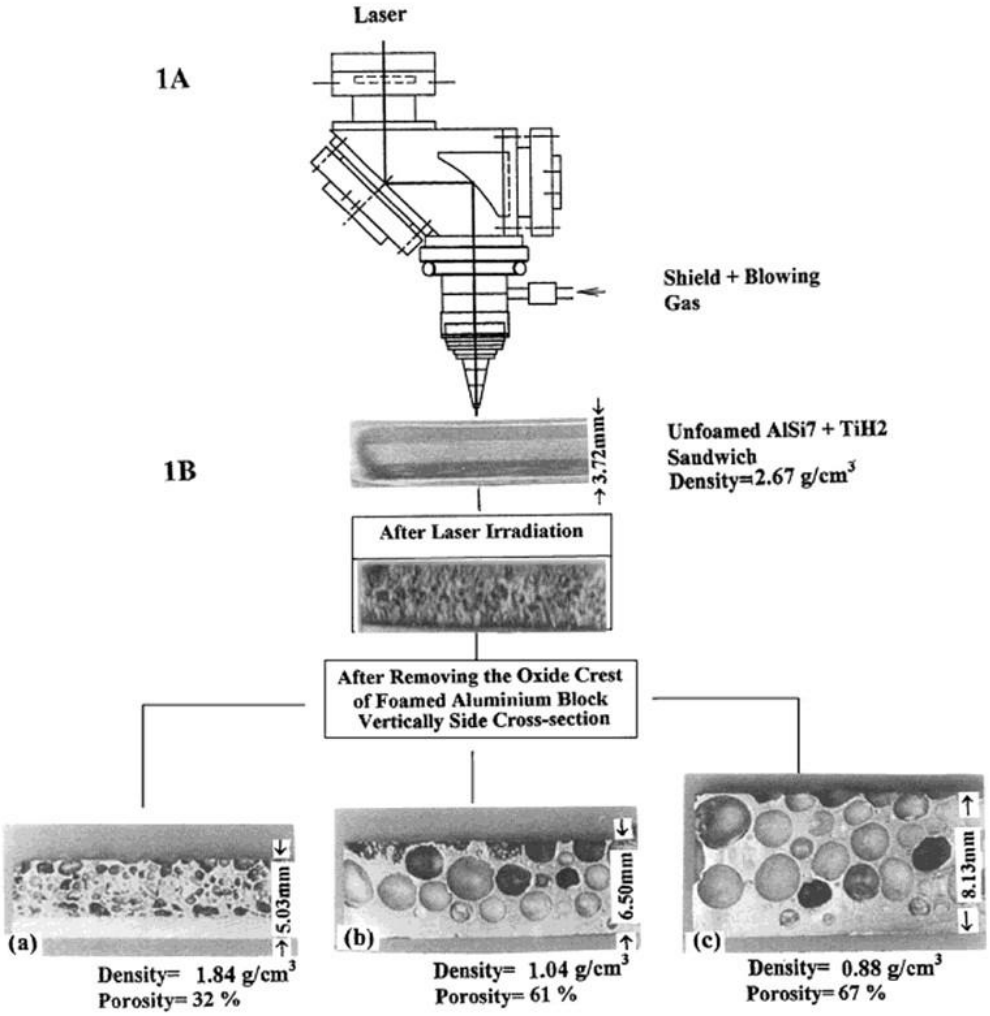


Figure 2.11. Schematic view of laser assisted foaming technique; processing speeds (V): (a): 2 m/min; (b): 0.8 m/min; (c): 0.4 m/min (Source: Kathuria 2003)

# CHAPTER 3

# MECHANICAL BEHAVIOR OF AL FOAMS

Under uniaxial compressive loads, Al closed cell foams show characteristic compressive stress strain behavior. The ideal compressive stress strain curve comprises three distinct deformation regions (Figure 3.1). In linear elastic region, the foam deformation is controlled by cell edge bending and/or cell face stretching. Collapse region occurs by highly localized cell edge buckling, crushing and tearing (Figure 3.2) (Gibson 2000). The collapse region is characterized by a collapse stress and/or a plateau stress either with a constant value or increasing slightly with strain (Figure 3.1). At a critical strain, $\varepsilon_d$, the cell walls start to touch each other and, as a result of this, the material densifies. The stress in this region increases sharply and approaches to the strength of the bulk Al metal.

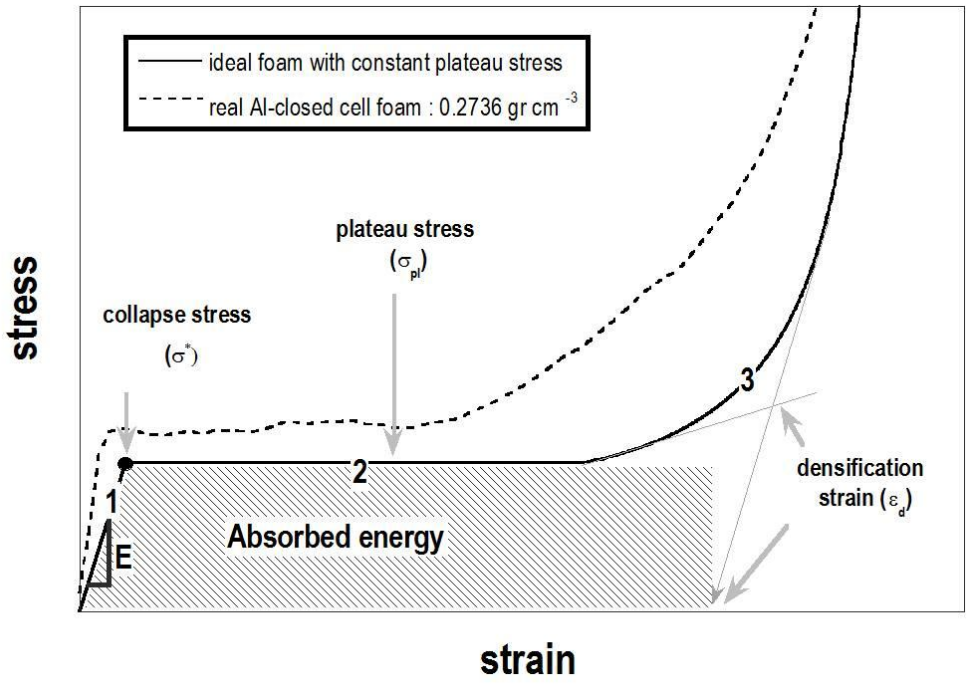


Figure 3.1. Compression stress strain curves of ideal foam and real Al-closed cell foam.

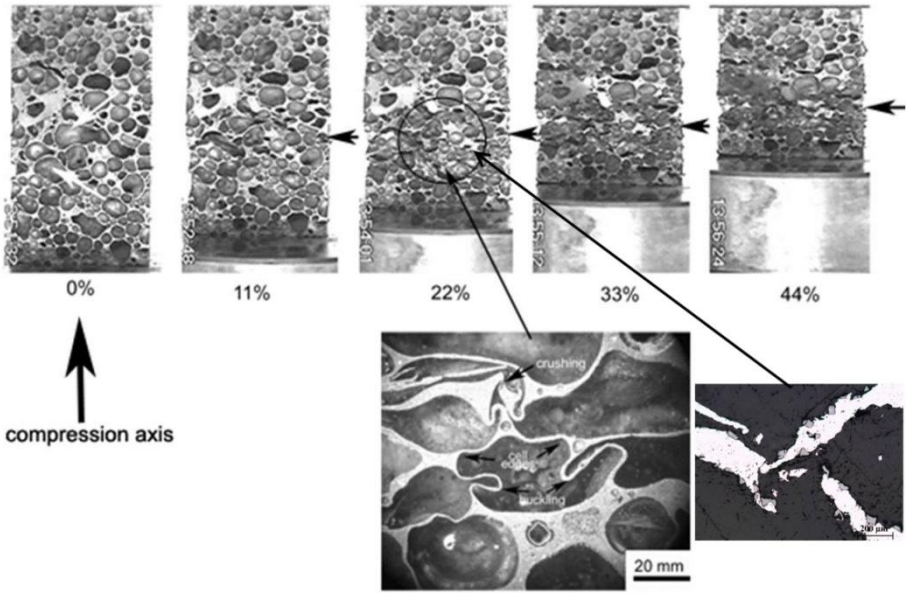


Figure 3.2. The deformation of highly localized Al foam sample at different strains and deformed foam cell structure in the localized deformed region. (Source: Guden and Yüksel 2006)

The elastic modulus ($E^*$) of ideal open and closed cell foams are calculated from the cell edge bending deflection and the stretching of the planar cell faces and is given sequentially as (Gibson and Ashby 1997),

$$\frac{E^*}{E_s} = c_1 \rho^2 \tag{3.1}$$

$$\frac{E^*}{E_s} = c_2 \rho^2 + c_3 \rho \approx c_4 \rho \tag{3.2}$$

where, $E_s$ is the elastic modulus of the cell wall material, $c_1$, $c_2$, $c_3$ and $c_4$ are the constants and $\rho$ is the foam relative density which is

$$\rho = \frac{\rho^*}{\rho_s} \tag{3.3}$$

where, $\rho^*$ is the density of foam and $\rho_s$ is the density of the cell wall material. For tetrakaidecahedral foams, $c_1 \sim 1$, $c_2=c_3 \sim 0.32$ and for low density foams, $c_4 \sim 0.32$ (Deshpande and Fleck 2000). The experimentally measured elastic moduli data in Figure (3.3(a)) are shown to present relatively good correlations with the open cell foam modulus values predicted by the Equations 3.1 and 3.2 (Gibson 2000).

The plateau stress determines the amount and efficiency of the energy absorption in the collapse region. For ideal open and close cell foams, the plastic collapse simply occurs by the plastic hinges at the bend cell edges and the cell wall stretching in perpendicular direction to the compression axis. Equations 3.4 and 3.5 relate sequentially the plateau stresses of ideal open-cell and tetrakaidecahedral closed-cell foams with relative density as,

$$\frac{\sigma_{pl}}{\sigma_{ys}} = 0.3\rho^{3/2} \tag{3.4}$$

$$\frac{\sigma_{pl}}{\sigma_{ys}} = 0.33\rho^2 + 0.44\rho \tag{3.5}$$

where, $\sigma_{pl}$ is the plateau stress and $\sigma_{ys}$ is the yield strength of the cell wall material. Relatively good correlations between the experimental relative compressive strength values of open and closed cell foams with compressive strength values predicted using Equation 3.4, which was developed for the open cell foams, was shown previously (Figure 3.3(b)). While, the experimental closed cell Al foam strength values showed deviations from the ideal strength data as depicted in Figure 3.3(b). This was attributed to the micro structural defects formed during manufacturing the closed cell foams including missing, fractured and bent cell walls and inhomogeneous cell wall allocations between cell walls and cell edges (Hall, et al. 2000). The defects may produce premature bending leading to the initiation of a deformation band in the foam.

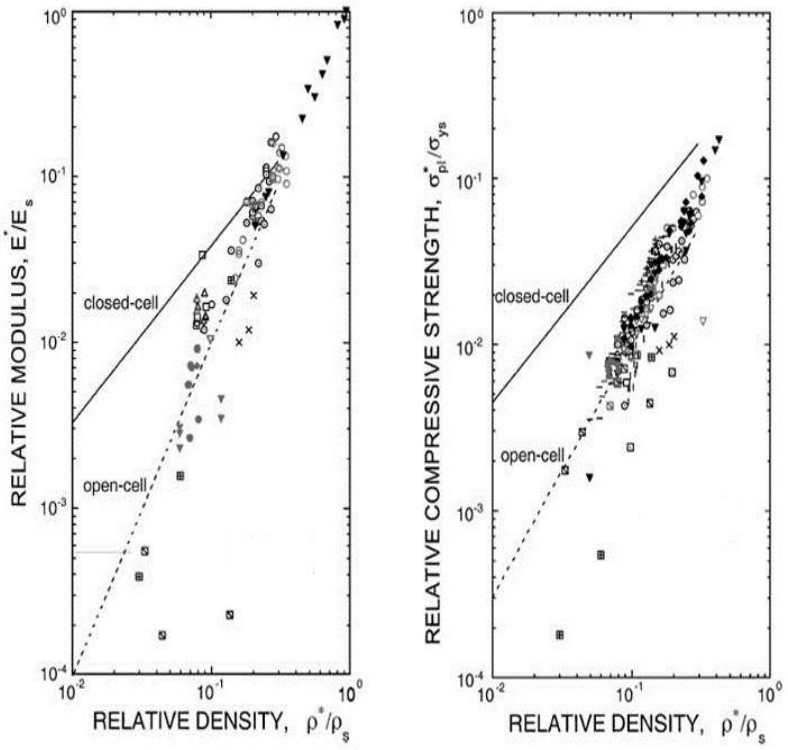


Figure 3.3. a) Relative modulus vs. relative density and b) relative compressive strength vs. relative density graphics of open and closed cell Al foam. (Source: Gibson 2000)

## 3.1. Rate Sensitivity of Cellular Materials

***Alulight IFAM foams produced through powder route:*** The mechanical behavior of IFAM closed cell foam (Al-Si) was previously investigated at quasi-static and high strain rates under compressive loads using quasi-static, drop weight and SHPB testing (Peroni, et al. 2008). It was reported that the foam showed no significant strain rate dependent yield stresses (collapse stress) within the investigated strain rate regime of $1x10^{-3}$ and 800 $s^{-1}$ and within the foam density range of 0.33 and 0.7 g $cm^{-3}$ (Figure 3.4). The quasi-static ($1x10^{-3}$ $s^{-1}$) and high strain rate (5000 $s^{-1}$) compressive behavior of closed-cell Alulight foam (Al-Mg0.6-Si0.3) and open cell Duocel Al6061-T6 were investigated (Deshpande and Fleck 2000). It was shown that no increase in the dynamic collapse stresses of both foams as compared those of quasi-static collapse stresses within the studies strain rate range and foam relative densities (Figure 3.5). The quasi-static and high strain rate compression behavior of Al6061-T6 IFAM foam with the strain rate regime of $1x10^{-3}$ and 2000 $s^{-1}$ and foam density range of 0.31 and 0.84 g $cm^{-3}$

were investigated. The foam showed no strain rate dependence in collapse stress (Figure 3.6) (Hall, et al. 2000). In an another study, the quasi-static and high strain rate compression behavior of AA6061 IFAM foams at 0.01 m $s^{-1}$ and 10 m $s^{-1}$ impact velocities with the foam density of 0.6 g $cm^{-3}$ were investigated. The results showed a strain rate dependent collapse stress; the dynamic collapse stress was %18 higher than those of quasi-static (Zhao, et al. 2005).

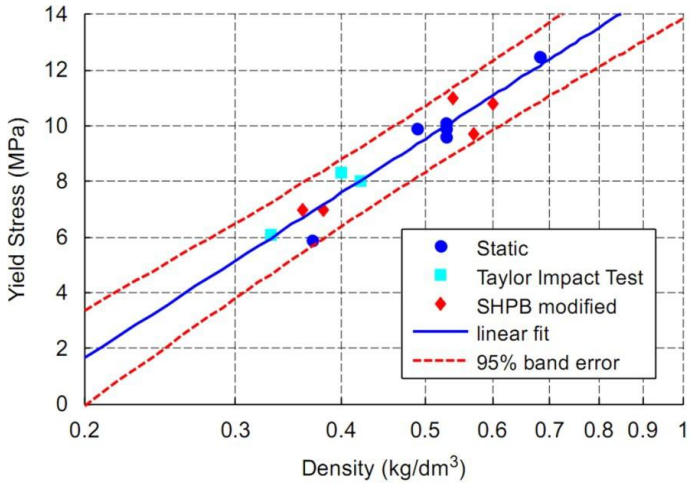


Figure 3.4. Strain rate sensitivity of Alulight closed cell foam.
(Source: Peroni, Avalle et al. 2008)

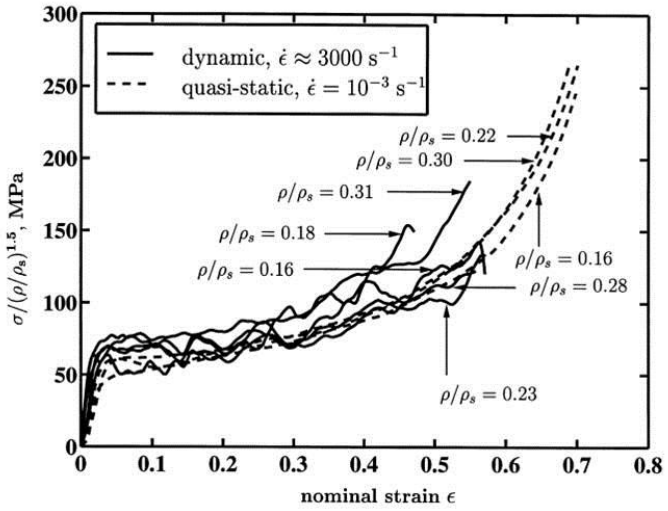


Figure 3.5. The effect of strain rate on the collapse behavior of Alulight closed cell foams up to 3000 $s^{-1}$. (Source: Deshpande and Fleck 2000)

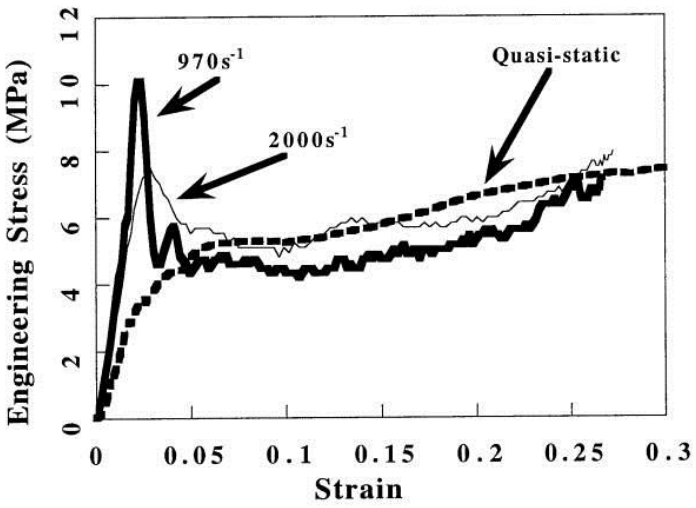


Figure 3.6. Strain rate dependence of 6061-Al foam
(Source: Hall, Guden et al. 2000)

***Alporas foams produced through melt route:*** The quasi-static and high strain rate compression behavior of Alporas foams of varying densities and at varying strain rates were investigated by several different investigators (Miyoshi, et al. 2000, Mukai, et al. 1999, Mukai, et al. 2006, Paul and Ramamurty 2000). It is found that the foam shows a strain rate dependent collapse and plateau stress as depicted in Figure 3.7.

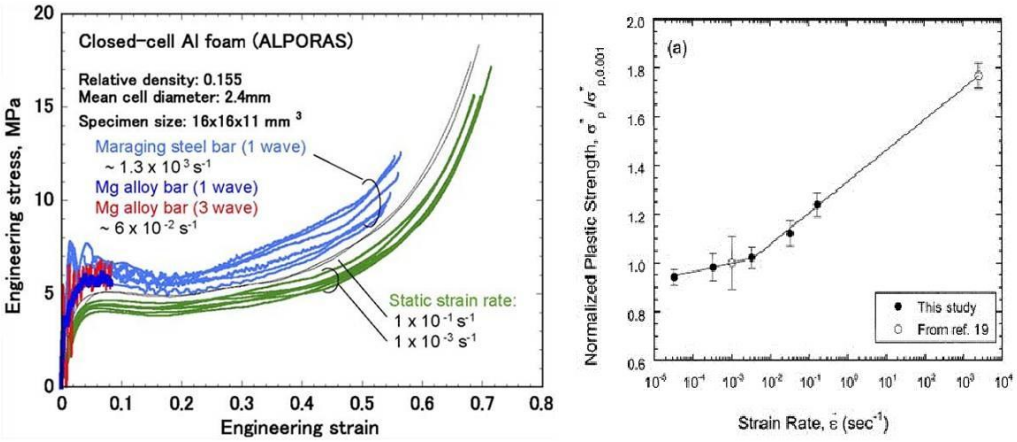


Figure 3.7. Strain rate sensitivity of Alporas closed cell Al foams
(Source: Mukai, Kanahashi et al. 1999, Paul and Ramamurty 2000)

***Cymat foams produced through melt route with ceramic particle addition:*** Cymat Al foams of 0.31 and 0.17 g $cm^{-3}$ and 15% SiC particle addition were tested at the strain rates between $1x10^{-3}$ and 100 $s^{-1}$. It was shown that strain rate had little effect on the mechanical properties of the foams (Kenny 1996). A similar strain rate independent plateau stress was also shown in an another study for Cymat foam with a density of 0.25 g $cm^{-3}$ (Zhao, et al. 2005).

The strain rate sensitive crushing stresses of cellular materials may results from the strain rate sensitivity of the cell wall, the micro-inertial effects, shock wave propagation and the compressed air pressure in the cells (Zhao, et al. 2005). The compressed air pressure in dynamic loading was shown to be less than 1.5% of the quasi-static strength of closed-cell Al foam (Deshpande and Fleck 2000). At increasing deformation velocities, excess of 50 m $s^{-1}$, shock wave propagation was shown to have a significant contribution to the strength of the cellular metallic structures (Reid and Peng 1997). In SHPB testing the deformation velocities, however, range between 5-10 m $s^{-1}$; therefore, the shock-wave propagation enhancement is usually ignored within the strain rate regime of the SHPB testing.

## 3.2. Micro Inertial Effect

Micro-inertial effects arise due to lateral inertia which results in increase of the buckling loads at increasing strain rates (Calladine and English 1984). Lateral inertia causes the buckling of a column under impact compression at a delayed time, so that the critical buckling force is higher than the quasi-static one. Even there is no wavelength change; the strength enhancement is still possible in progressive folding because of inertia effects.

Micro-inertia, the columnar structures are classified in two groups: Type I and Type II structures (Calladine and English 1984). Type I structures are characterized with a flat-topped quasi-static load deflection curve (Figure 3.8), showing limited or no strength enhancement at increasing deformation velocities. Type II structures are characterized with a strong softening after yielding at quasi-static strain rates and the lateral inertia forces lead to increased bending forces at increasing deformation velocities. Examples for type II structures include axially loaded columns. The increased deformation forces at increasing strain rates in the compression of Al

honeycomb structures through out of plane (Zhao, et al. 2005), metallic columnar structures (Langseth and Hopperstad 1996), Al foams ((Lee, et al. 2006), (Paul and Ramamurty 2000), (Zhao, et al. 2005)) and balsa wood in the axial direction ((Reid and Peng 1997), (Tagarielli, et al. 2008)) were reported to result from the micro-inertial effects.

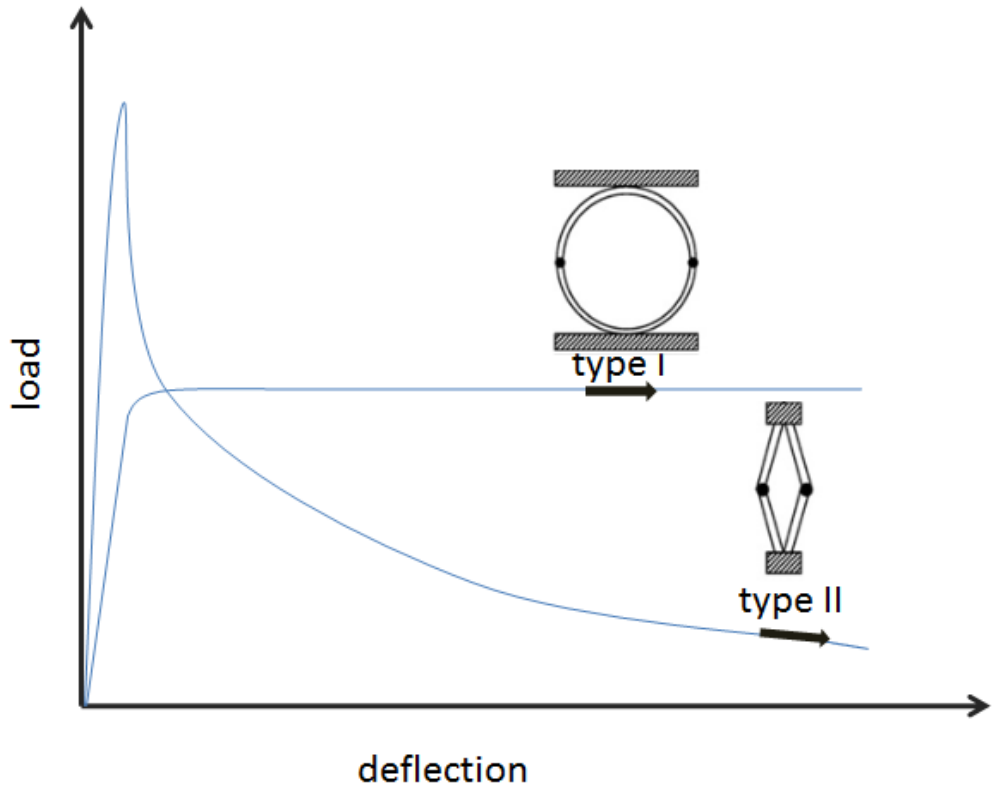


Figure 3.8. Type I and Type II structures
(Source: Calladine and English 1984)

The dynamic out-of-plan behaviors of 5056 and 5052 Al honeycombs were studied and typical progressive buckling pattern observed for all Al honeycombs (Zhao, et al. 2006). Figure 3.9 shows 15% stress enhancement in dynamic loading in honeycombs. This enhancement is not due to the air pressure and inertia effect in the progressive folding process is supposed to be the main origin rather than the strain rate sensitivity of the base material, as Al is not a strain sensitive material. The IFAM AA6061 foams were obtained from AA6061 Al powder and 0.5 wt.% titanium hydride powder with Al powder blowing process. The test results gave the enhancement of 15%

for mean flow stress as seen in Figure 3.10 and it is supposed to the micro-inertia effect because of the progressive folding of the cell wall. Static and dynamic loading tests were applied to the Cymat foam which was manufactured by gas injection method. In Figure 3.11, there is no difference between static and dynamic mean stress and nominal strain curves, proofing that the base material sensitivity of Al and air pressure does not play a significant role. Since fracture occurred on the cell wall, the inertia effect did not involve in the successive folding. Since the buckling of cell walls is the dominant micro-mechanism of the deformation in the foams, micro-inertial effects are thought to be the cause for the observed enhancement.

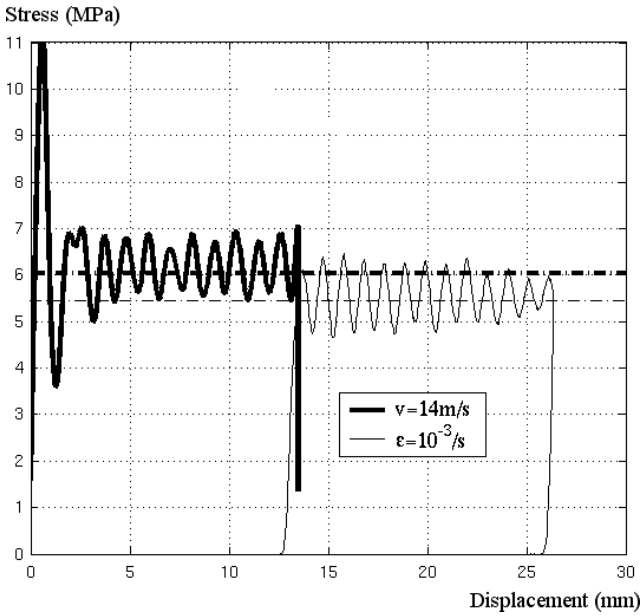


Figure 3.9. A typical mean stress- displacement curve during impact and subsequent quasi-static tests. (Source: Zhao, Elnasri et al. 2006)

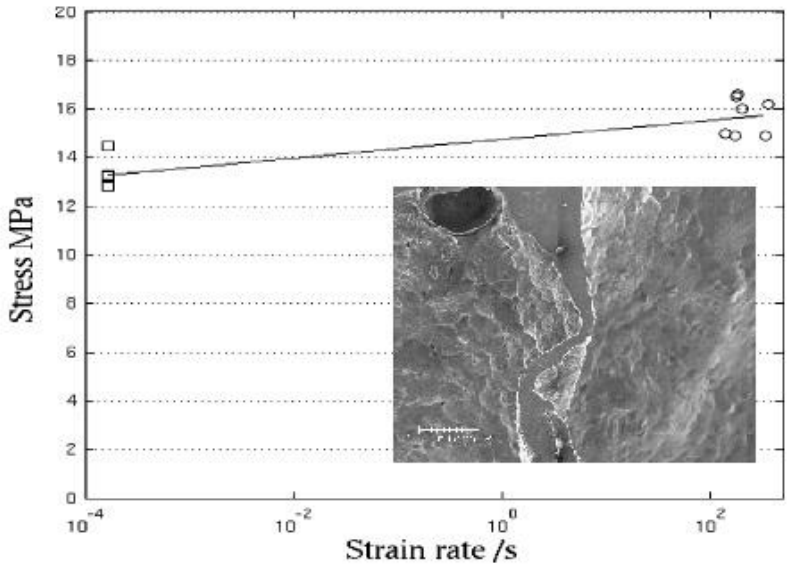


Figure 3.10. Rate sensitivity of foams and progressive folding of cell walls (Source: Zhao, Elnasri et al. 2006)

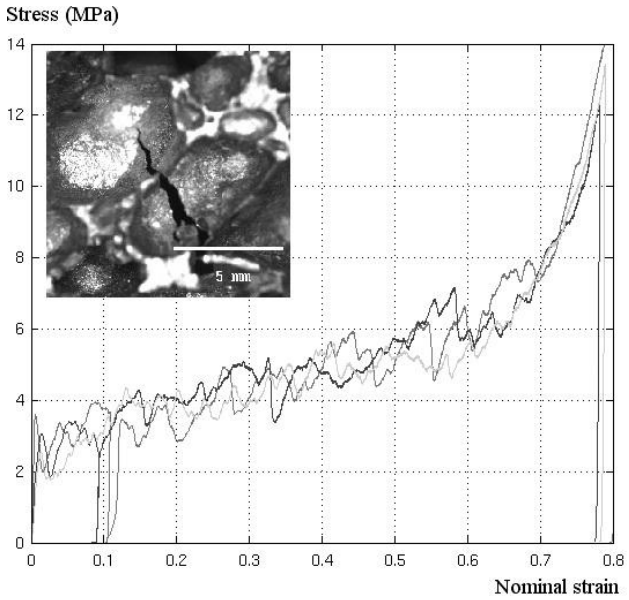


Figure 3.11. Mean stress vs. nominal strain curves under quasi-static and dynamic loading and failure mode of brittle Cymat foam. (Source: Zhao, Elnasri et al. 2006)

Shen and Lu (Shen, et al. 2010) schematized the plastic deformation mechanisms for low and high strain rate loadings as a result of micro-inertia of cell walls. Plastic deformation mechanism changes as a result of micro-inertia of the cell walls. It is well known that when the impact velocity is sufficiently high, the deformation mechanism changes, with the position of some plastic hinges being closer to the loading point; a possible scenario is also shown in Figure 3.12. This will lead to a very different, much less compact configuration at the end of deformation. Hence the densification strain will be less than the quasi-static case ($1x10^{-3}s^{-1}$).

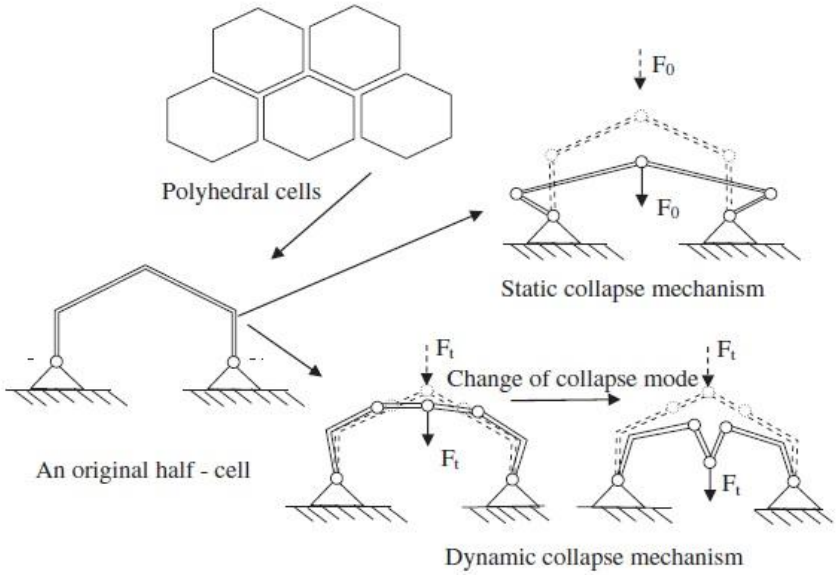


Figure 3.12. Plastic deformation mechanisms.
(Source: Shen et al. 2010)

The energy-deflection curves for two idealized types of structures shown in Figure 3.13(a) and (b) are drawn according to the following formulas;

$$Type-I: U = C_1 s \tag{3.6}$$

$$Type-II: U = C_2 s^{1/2} \tag{3.7}$$

By using Equation (3.6) and Equation (3.7), load-deflection curves are drawn according to;

$$Type-I: F = dU/ds = C_1 \tag{3.8}$$

$$Type-II: F = dU/ds = \frac{1}{2} C_2 s^{-1/2} \tag{3.9}$$

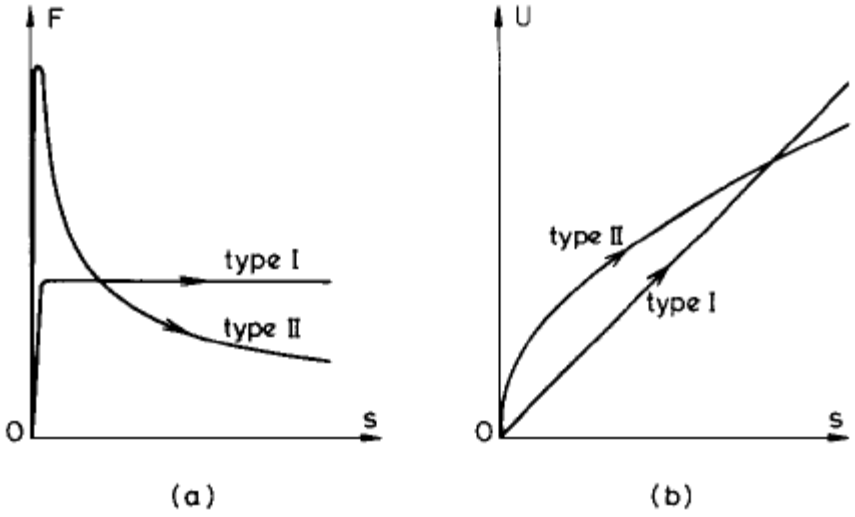


Figure 3.13. (a) Load-deflection and (b) energy-deflection curves for idealized Type-I and Type-II structures under quasi-static conditions. (Source: Calladine and English 1984)

In a standard quasi-static test, absorption energy $U_o$ is a result of total displacement of $s_o$. So, Equation (3.6) and Equation (3.7) can be written as;

$$Type-I: \frac{U}{U_o} = \frac{s}{s_o} \tag{3.10}$$

$$Type-II: \frac{U}{U_o} = (\frac{s}{s_o})^{1/2} \tag{3.11}$$

The yield stress ($\sigma_y$) is given as,

$$\frac{\sigma_y}{\sigma_o} = 1 + (\frac{\dot{\varepsilon}}{\dot{\varepsilon}^*})^a \tag{3.12}$$

where, $\sigma_o$ is the quasi-static yield stress, $\dot{\varepsilon}$ is the current strain rate, $\dot{\varepsilon}^*$ is the reference strain rate and a is a constant. By using the following function

$$f(x) = 1 + x^a \tag{3.13}$$

equations may be arranged as,

$$\frac{\sigma_y}{\sigma_o} = f(\frac{\dot{\varepsilon}}{\dot{\varepsilon}^*}) \tag{3.14}$$

and,

$$\frac{\sigma_o}{\sigma_y} = \frac{1}{f(\dot{\varepsilon}/\dot{\varepsilon}^*)} \tag{3.15}$$

In an impact test, the deformation due to the moving mass can be written as;

$$\dot{\varepsilon} = CV_o \tag{3.16}$$

where, C is constant and $V_o$ is the velocity. In terms of strain rates, following relations may be obtained

$$\frac{\dot{\varepsilon}}{\dot{\varepsilon}^*} = \frac{V_o}{V^*} \tag{3.17}$$

Hence;

$$\frac{\sigma_o}{\sigma_y} = \frac{1}{f(V_o/V^*)} \tag{3.18}$$

In an artificial quasi-static test, the final displacement can be replaced by actual quasi-static yield stress and total displacement can be thought as equivalent in terms of deflection to a quasi-static test at the quasi-static yield stress, $\sigma_o$, but with a reduced energy input, $U_r$.

$$\frac{U_r}{U_o} = \frac{\sigma_o}{\sigma_y} \tag{3.19}$$

Then, Equation 3.10 and Equation 3.11 may be written as respectively,

$$Type - I: \frac{s}{s_o} = \frac{1}{f(V_o/V^*)} \tag{3.20}$$

$$Type - II: \frac{s}{s_o} = \left[\frac{1}{f(V_o/V^*)}\right]^2 \tag{3.21}$$

To conclude, s is much more sensitive to $V_o$ for Type II structures than for Type I structure.

# CHAPTER 4

# EXPERIMENTAL DETAILS AND SAMPLE PREPARATION

## 4.1. Quasi-static Testing

Quasi-static compression tests were performed using a displacement-controlled SHIMADZU AG-300kNX universal tension-compression test machine at Dynamic Testing and Modeling Laboratory of İzmir Institute of Technology (Figure 4.1). Compression tests data were digitally recorded including time, load and displacement. Load and displacement data were then used to determine the stress-strain curves of the tested specimens. The compression tests were conducted between tool steel compression test plates. Before the test, the surfaces of the plates were lubricated in order to reduce frictional forces between plates and specimen surfaces. The quasi-static compression tests were performed at two different strain rates, $1x10^{-3}$ $s^{-1}$ and $1x10^{-1}$ $s^{-1}$. In the quasi-static tests at the strain rate of $1x10^{-3}$ $s^{-1}$, the test cross-head speed increased 100 times, corresponding to a strain rate of $1x10^{-1}$ $s^{-1}$ at a prescribed strain. These tests were called *reloading tests*. Reloading tests were performed in order to see the effect of strain rate on the test material without stopping the test. Therefore, any material inhomogeneity that may affect the strength of the test material is excluded in the strain rate sensitivity analysis.

In the thesis, the following materials were tested: Al tubes, Al foam with/without SiC particles, corrugated Al structures and brittle glass foam. At least three compression tests were performed for each group of material. The nominal strain and stress in the compression test were calculated using the following relations:

$$\varepsilon = \frac{\delta}{Lo} \tag{4.1}$$

$$\sigma = \frac{P}{Ao} \tag{4.2}$$

where, δ is the displacement, P is the load, $L_o$ is the initial length and $A_o$ is the cross-sectional area of the tested specimen. The strain rate was calculated as,

$$\dot{\varepsilon} = \frac{c}{L_0} \tag{4.3}$$

where, c is the displacement rate or cross-head speed.

Figure 4.1. Static test machine (SHIMADZU AG–300kNX).

## 4.2. High Strain Rate Testing

High strain rate tests were conducted using a SHPB set-up at Dynamic Testing and Modeling Laboratory of İzmir Institute of Technology. The SHPB set-up and SHPB schematic are further shown in Figure 4.2 and Figure 4.3, respectively. In a typical test, pressurized gas gun fires the striker bar onto the incident bar with an initial velocity of $v_o$. Striker bar impact to end of the incident bar forms a compressive elastic stress wave on the incident bar. The amplitude of the wave created is directly related with the speed of the striker bar. This wave propagates through the incident bar until the specimen bar interface. At the specimen bar interface, a part of the wave transmitted to the specimen and other part is reflected back. Incident and reflected strains are measured by the gage on the incident bar and the transmitted strain is measured by the gage on the transmitter bar. These gages are connected to the strain gage conditioner in which the voltage signal is amplified. An oscilloscope is used to monitor and store the strain-time data. The stress, strain and strain rate values are calculated using the following equations:

$$\sigma(t) = \frac{E_b A_b}{A_s} \varepsilon_t(t) \tag{4.4}$$

$$\varepsilon(t) = \frac{-2C_b}{L_s} \int_0^t \varepsilon_r(t)\, dt \tag{4.5}$$

$$\dot{\varepsilon}(\mathrm{t}) = \frac{-2C_b}{L_s} \varepsilon_r(t) \tag{4.6}$$

where, $E_b$ is the elastic modulus of the bar, $A_b$ is the cross-sectional area of the bar, $A_s$ is the cross-sectional area of the specimen, $L_s$ is length of the specimen, $C_b$ is the wave velocity of the bar, $\varepsilon_t(i)$ is the incident strain history, $\varepsilon_t(t)$ is the transmitted strain history and $\varepsilon_r(t)$ is the reflected input bar strain history.

Figure 4.2. SHPB apparatus in DTM Lab at IZTECH.

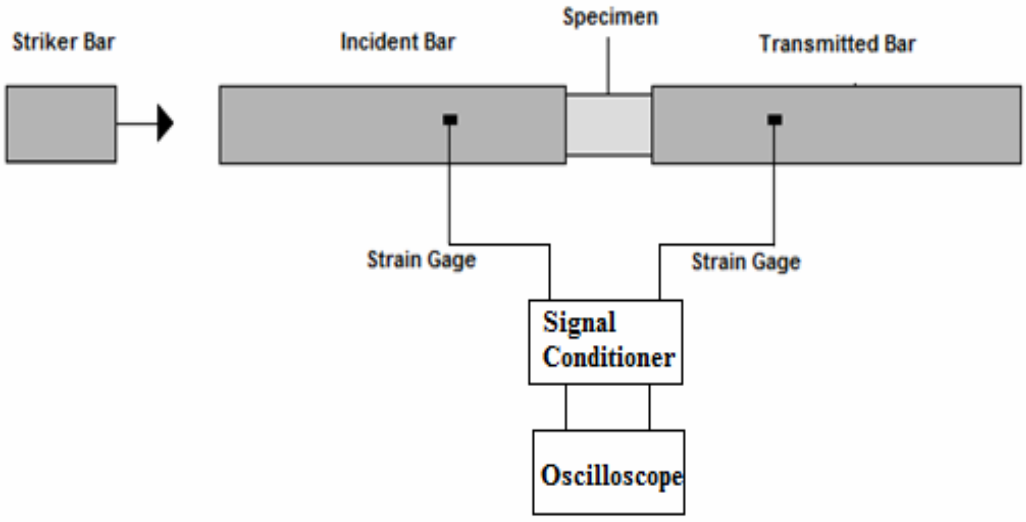


Figure 4.3. Schematic of Split Hopkinson Pressure Bar.

In developing SHPB equations, the forces at specimen-bar interfaces are assumed to be equal as,

$$\sigma_t(\mathrm{t}) = \sigma_i(\mathrm{t}) + \sigma_r(\mathrm{t}) = \frac{\sigma_t(\mathrm{t})+\sigma_i(\mathrm{t})+\sigma_r(\mathrm{t})}{2} \tag{4.7}$$

$$\sigma(t) = \frac{E_b A_b}{A_s}\varepsilon_t(t) = \frac{E_b A_b}{A_s}(\varepsilon_i + \varepsilon_r)(t) = \frac{E_b A_b}{2A_s}(\varepsilon_i + \varepsilon_r + \varepsilon_t)(t) \tag{4.8}$$

The first, second and third term of the Equation 4.7 are called one-wave, two-wave and three-wave analyses, respectively. Stress equilibrium is considered to be reached after 3–4 back and forth reflections of the wave in the sample and the time at which equilibrium is established depends on the wave transit time of the sample. Cylindrical test samples used in SHPB tests were 19 mm in diameter and length with an l/d ratio of 1.5. A thin grease layer was applied on both interfaces of the bars before the cylindrical samples were sandwiched between the incident and transmitter bars to minimize the frictional forces. The SHPB apparatus used consists of Inconel 718 bars, 500 mm striker, 3116 mm incident and 2080 mm transmitter bars, all with a diameter of 19.35 mm. The samples tested quasi-statically until about a prescribed strain were also tested in SHPB in order to see the effect of strain on the deformed samples. These tests are called static-dynamic reloading tests.

## 4.3. Materials

The tested deep-drawn Al tubes were produced by METALUM Company of Turkey and received in diameter of 25 mm and having wall thickness of 0.29 mm (Figure 4.4). The tubes were cut in 25 mm pieces using a diamond cutting machine. The quasi-static compression tests were conducted through axial and transverse directions.

Figure 4.4. Empty Al tube.

Aluminum closed cell foams were prepared using the foaming from powder compacts (precursors) process, patented by Fraunhofer CMAM (Baumeister and Schrader 1992). The process was started with the mixing of appropriate amounts of basic ingredients, Al powder, $SiC_p$ (15 wt%) and $TiH_2$ (1 wt%), inside a plastic container, which was rotated on a rotary mill in order to form a homogeneous powder mixture (Figure 4.5). The average particle size of the Al and $SiC_p$ were 34.64 and 22.36 μm, respectively and the size of $TiH_2$ particles was less than 37 μm. The specification of raw materials used is given elsewhere.

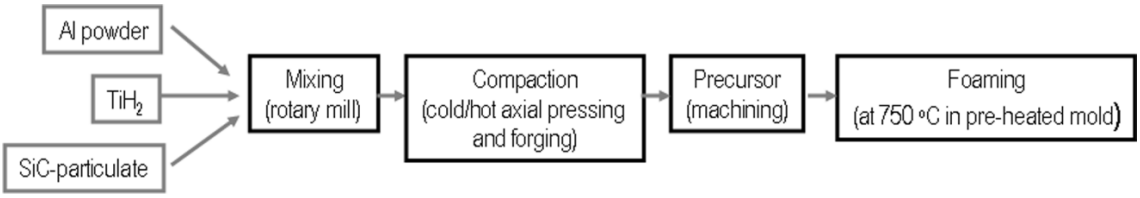


Figure 4.5. The processing stages of the foaming process.

The powder mixture was initially cold compacted inside a steel die, 70x70 cm in cross-section, under a pressure of 200 MPa. The compacts having 80% relative density were then open-die hot-forged at a temperature of 350 $^{o}$C, resulting in foamable precursor materials with the final densities of 98% and thicknesses of approximately 8 mm. As a result of open die forging, the cross-sectional area of the precursor increased and small cracks were formed at the edges of the precursor. Foaming experiments were conducted in a pre-heated furnace at a temperature of 750 $^{o}$C (Figure 4.6). The precursor was inserted into a pre-heated steel mold providing expansion only in the vertical direction (Figure 4.7). After precursor insertion, the steel mold (closed at the bottom) was closed at the top (Figure 4.7). The inserting and removing specimen took less than 10 seconds. The precursor started to expand after 5 min and filled the die completely at about 7 min (Figure 4.8). The cut foam samples were individually weighed and measured in order to

calculate relative densities before compression testing. The relative density, $\rho^*$, is calculated as

$$\rho^* = \frac{\rho_f}{\rho_s} \tag{4.9}$$

where, $\rho_f$ and $\rho_s$ refer to the foam and bulk alloy densities, respectively. The cylindrical foam test samples were prepared through core drilling as shown in Figure 4.9.


Figure 4.6. Foaming furnace, hot mold carrier and foaming mold.

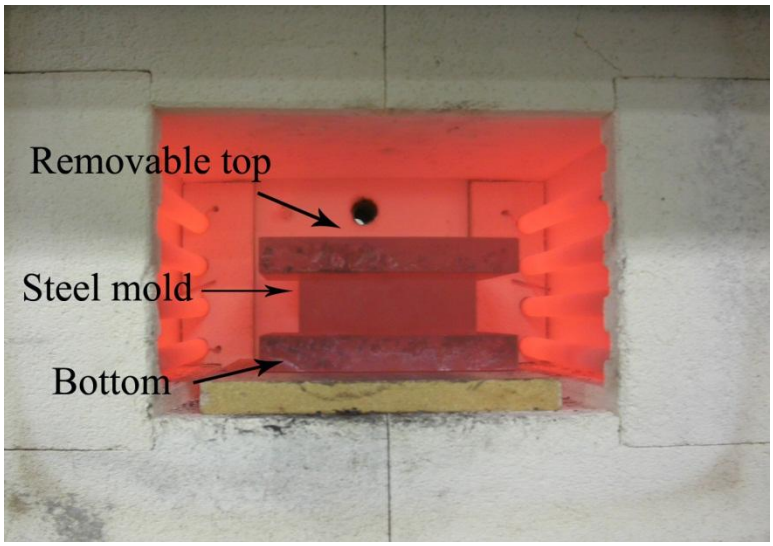


Figure 4.7. Foaming in the furnace with a steel mold closed at the top and bottom.

Figure 4.8. Foamed precursor that completely filled foaming the mold.

Figure 4.9. Al foam test sample with SiC particles.

As received Alulight Al (AlSi10) closed cell foam panels were received in 625x625x30 mm size. The panels accommodated relatively dense Al layer at the edges and the corners. Before the preparation of tests samples, the dense Al regions near the edges and corners of the panels were removed using a decoupling machine. Later, cylindrical compression test samples were core-drilled.

The corrugated Al structures including face sheets, interlayer sheets and core were made of 1050H14 Al alloys. The corrugated structures were prepared by bonding the individual layers (fin, interlayers and face sheets) using an epoxy glue. The thicknesses of 1050H14 alloy were 0.135 mm in the fin and 2 mm in the face sheets. The trapezoidal corrugated Al layers used to construct core material in the sandwich structure were produced using a sheet folding process. The folding was accomplished using a paired punch and die tool to fold Al sheets into regular trapezoidal core resulting in a highly flexible core structure. The details of the corrugated structure preparation is found in (Odacı 2011).

Each type of Al sandwich plate was tested at quasi-static strain rates and reloaded at quasi-static strain rates. Reloading was applied after compressing 40% of the original height of the specimen. The prepared and tested specimens are as follows:

***20 mm Thick $0^o/0^o$ Al Sandwich Plate:*** Two 8.5 mm thick Al fin plates combined together in $0^o/0^o$ orientation and 1mm thick of Al sheets were used between the layers and as face sheets (Figures 4.10(a) and (b)).

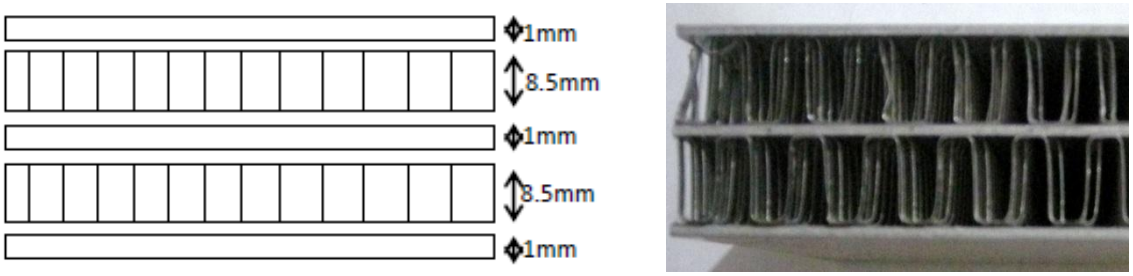


(a) (b)

Figure 4.10. 20 mm thick, $0^o/0^o$ Al sandwich plate; (a) schematic and (b) picture.

***20 mm Thick $0^o/90^o$ Al Sandwich Plate:*** Two 8.5 mm thick Al fin plates combined together in $0^o/90^o$ orientation (Figures 4.11(a) and (b)). This structure has the same fin layer with 20 mm thick, $0^o/0^o$ Al sandwich plate except fin layer orientation.

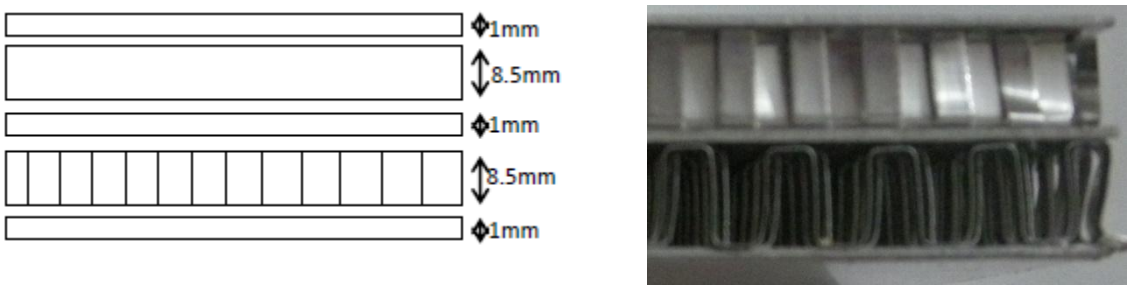


(a) (b)

Figure 4. 11. 20 mm thick, $0^o/90^o$ Al sandwich plate; (a) schematic and (b) picture.

***28mm Thick $0^o/0^o$ Al Sandwich Plate:*** Two 12.5 mm thick Al fin plates glued together in of $0^o/0^o$ orientation (Figures 4.12(a) and (b)).

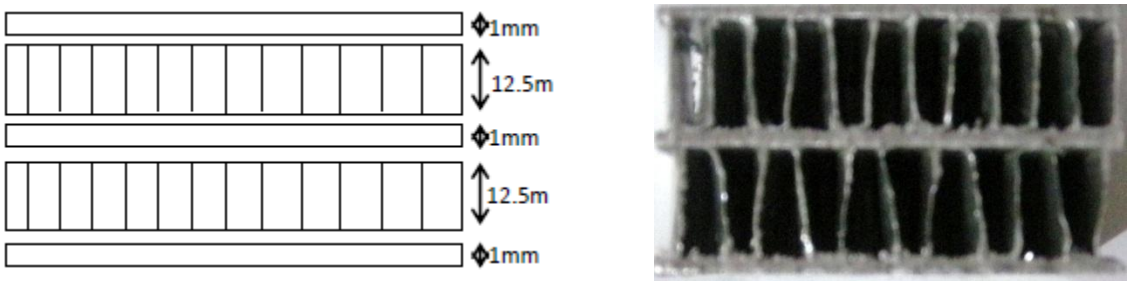


(a) (b)

Figure 4.12. 28 mm thick, $0^o/0^o$ Al sandwich plate; (a) schematic and (b) picture.

***28 mm Thick $0^o/90^o$ Al Sandwich Plate:*** Two 12.5mm thick Al fin plates combined together in the orientation of $0^o/90^o$ (Figures 4.13(a) and (b)). This structure has the same fin layer with 28 mm thick, $0^o/0^o$ Al sandwich plate except fin layer orientation.

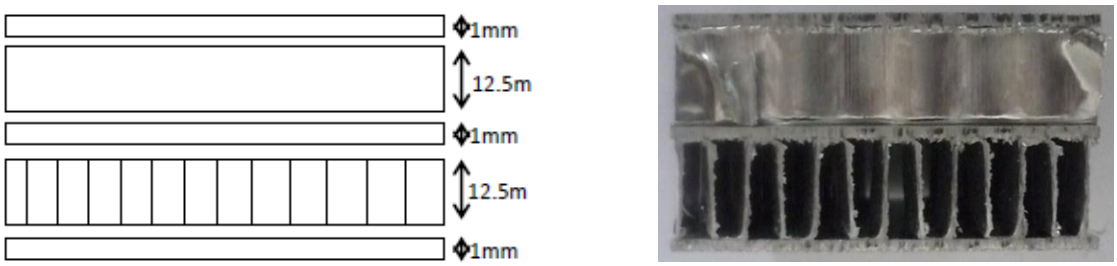


(a) (b)

Figure 4.13. 20 mm thick, $0^o/90^o$ Al sandwich plate; (a) schematic and (b) picture.

***42.5 mm Thick, $0^o/90^o$ Al Sandwich Plate:*** Thirteen 3 mm thick Al fin plates combined together in of $0^o/90^o$ orientation by brazing and 0.25mm thick of Al sheets were used between the layers and as face sheets as shown in Figures 4.14(a) and (b).

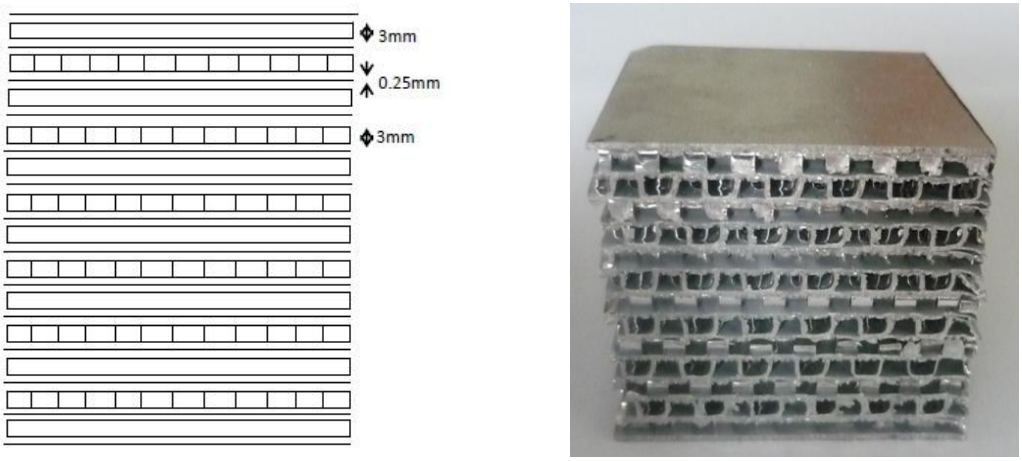


(a) (b)

Figure 4.14. 42.5 mm thick, $0^o/90^o$ Al sandwich plate; (a) schematic and (b) picture.

In order to show the effect of inertia on brittle foams, glass foam specimens were prepared and tested. The glass foam samples were prepared by mixing scrap glass powder of 200 μm with SiC powder of 70 μm and heating the mixture to 900 $^o$C for 15

minutes in a furnace in a mold. The percentage of SiC powder was 2 wt% and the mixture was pre-shaped in a rectangular mold of 8x8x4 cm at 40 MPa. The foam compression test samples, 22x22x22 mm in size (Figure 4.15) were cut from the rectangular foam sample

Figure 4.15. Glass foam test specimen.

# CHAPTER 5

# RESULTS AND DISCUSSIONS

## 5.1. Quasi-static Tests of Al Tubes

The load-displacement and displacement rate-displacement curves of the reloaded extruded Al tubes through lateral and axial directions are shown in Figures 5.1(a) and (b), respectively. As seen in the same figures, at a displacement of 8.7 mm, the tube displacement rate is increased from $1.6x10^{-3}$ to $1.6x10^{-1}$ mm $s^{-1}$. In the lateral direction, there is almost no increase in load values when the deformation rate is increased from $1.6x10^{-3}$ to $1.6x10^{-1}$ mm $s^{-1}$ (Figure 5.2a). On the other hand; the load increases about 66 N, when the deformation rate is increased from $1.6x10^{-3}$ to $1.6x10^{-1}$ mm $s^{-1}$ in the tube axial direction (Figure 5.2b). These confirm that tube lateral deformation reflects Type I and tube axial deformation reflects Type II structures as stated earlier. In Type I, micro-inertia plays little role under dynamic loading, while Type-II structures are inertia sensitive. A simple calculation shows that the rate of increase in the load is roughly 400 N $s^{-1}$ in the axial deformation of the tube.

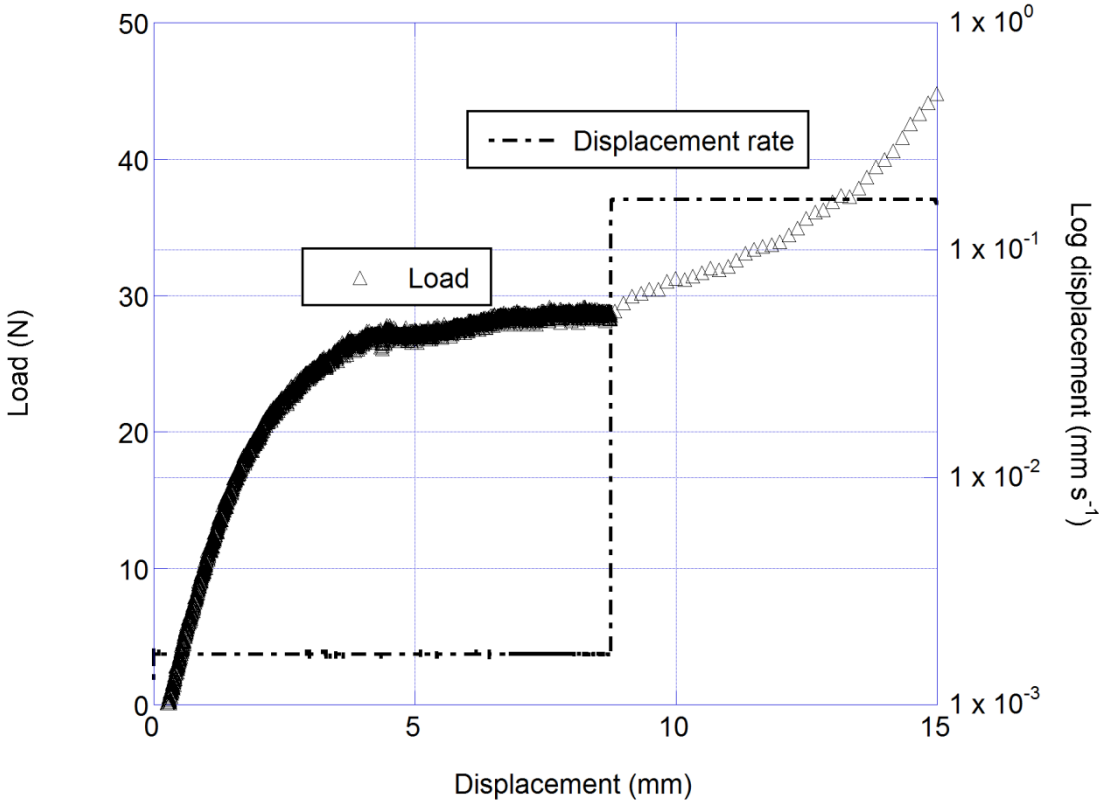


(a)

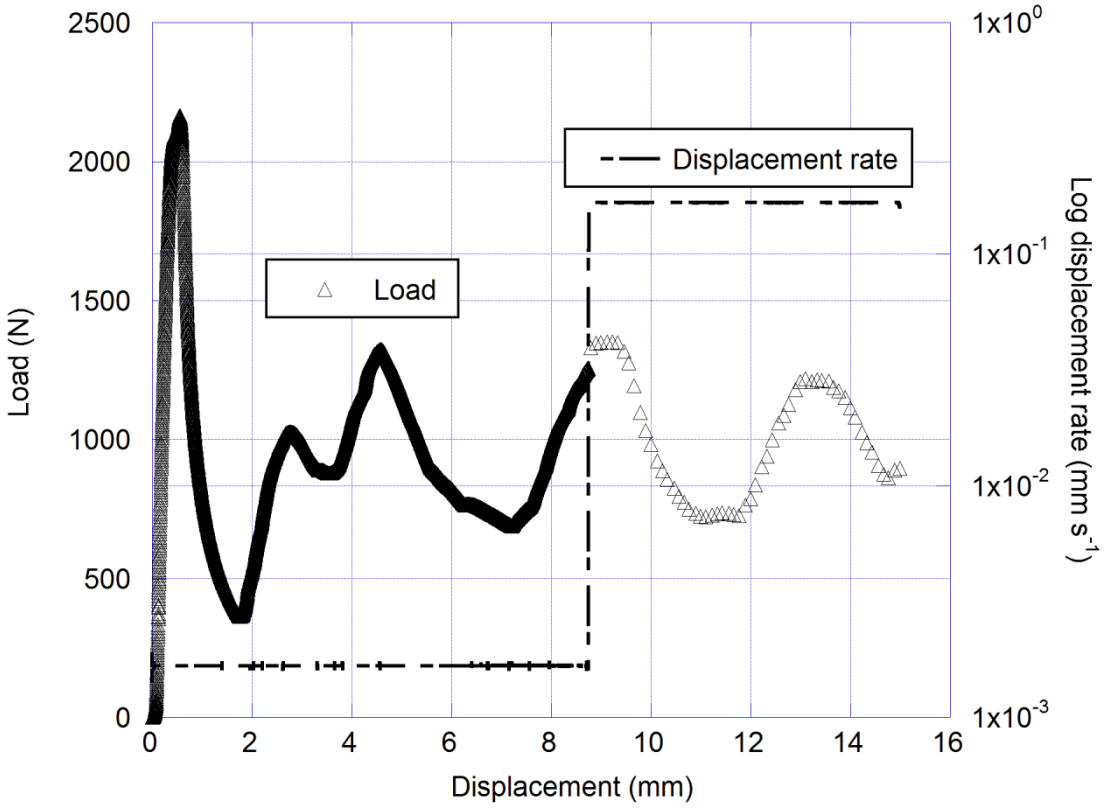


(b)

Figure 5.1. Reloading compression tests of Al tubes (a) lateral and (b) axial directions.

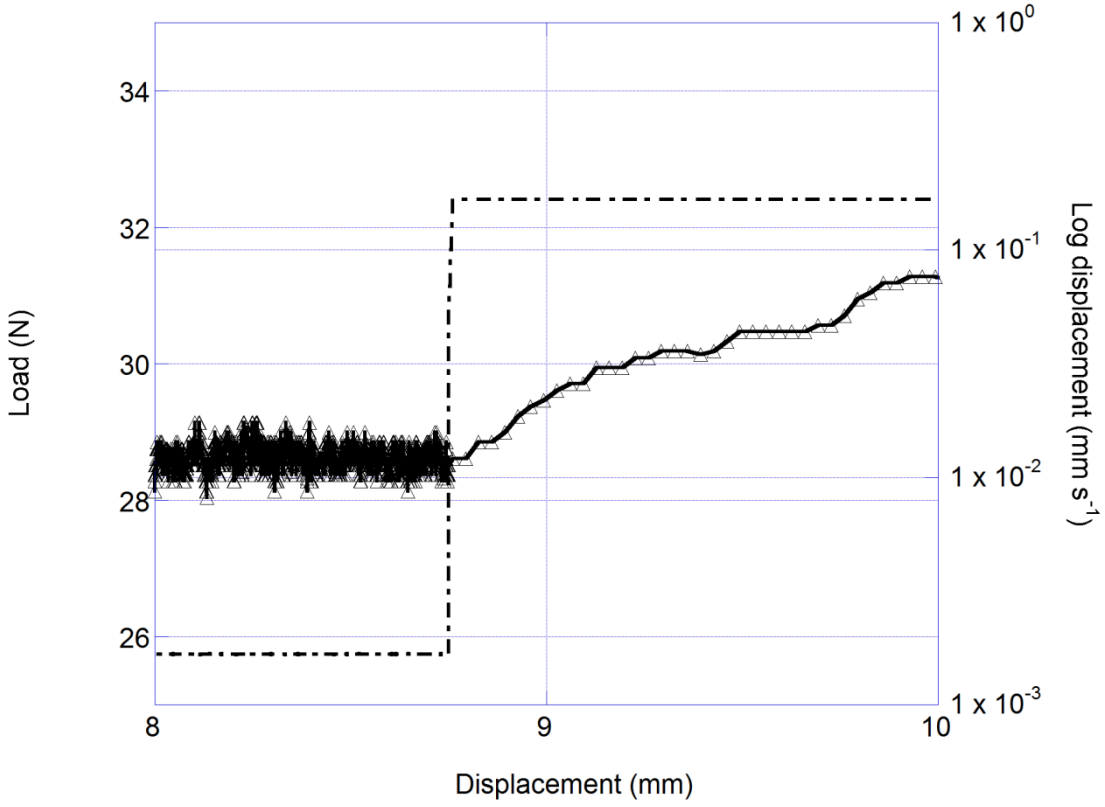


(a)

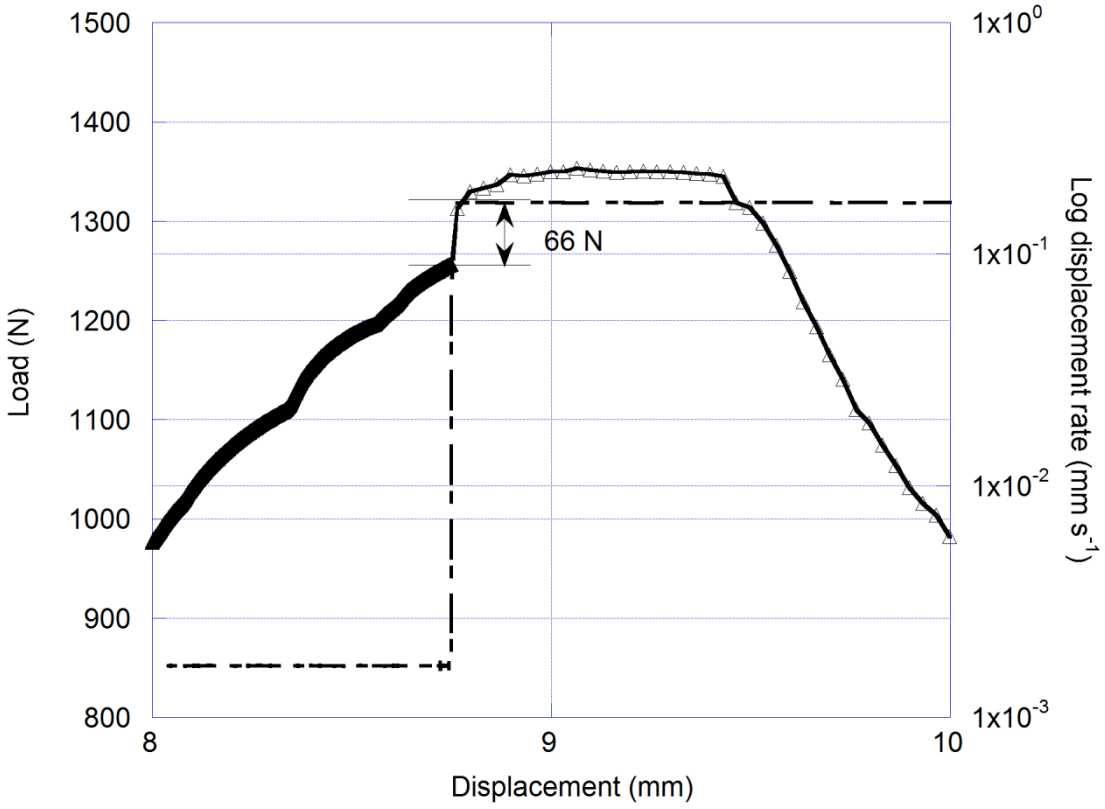


(b)

Figure 5.2. Magnified Al tube (a) lateral and (b) axial compression.

## 5.2. Quasi-static Tests of Al foams

The stress-strain and strain rate-displacement curves of the reloaded Al foams are shown in Figures 5.3(a) and (b). As seen in the same figures, at a strain of 0.2, the foam compression strain rate is increased from $1x10^{-3}$ to $1.0x10^{-1}$ $s^{-1}$. The circles in Figure 5.3(b) show the increase in stress values when the strain rate is increased from $1x10^{-3}$ to $1x10^{-1}$ $s^{-1}$. The foam tested show a strain rate sensitive compression behavior as depicted in the same figure. The average increase in the stress values is about 0.07±0.01 MPa when the strain rate is increased from $1x10^{-3}$ to $1x10^{-1}$ $s^{-1}$, corresponding to a stress increase rate of 0.707 MPa $s^{-1}$.

The stress-strain and strain rate-displacement curves of the reloaded Al/SiC foams are shown in Figures 5.4(a) and (b). As with Al foams, at a strain of 0.18, the foam compression strain rate is increased from $1x10^{-3}$ to $1x10^{-1}$ $s^{-1}$. The circles in Figure 5.4(b) show the increase in stress values when the strain rate is increased from $1x10^{-3}$ to $1x10^{-1}$ $s^{-1}$. The tested Al/SiC foams show a similar reloading behavior with Al foams, namely the stress values increase with increasing strain rate. The average increase in the stress values is about 0.078±0.01 MPa when the strain rate is increased from $1x10^{-3}$ to $1x10^{-1}$ $s^{-1}$, corresponding to a stress increase rate of 0.78 MPa $s^{-1}$. It is noted that the stress increase rate of Al and Al/SiC foams are very similar and show a similar response to the reloading.

The stress-strain and strain rate-displacement curves of the reloaded Alulight Al (AlSi10) closed cell foams are shown in Figures 5.5(a) and (b). As with Al foams, at a strain of 0.2, the foam compression strain rate is increased from $1x10^{-3}$ to $1x10^{-1}$ $s^{-1}$. The circle in Figure 5.5(b) show the variations of the stress values when the strain rate is increased from $1x10^{-3}$ to $1x10^{-1}$ $s^{-1}$. Different from the tested Al foams, Alulight foams show almost no strain rate sensitive behavior as depicted in Figure 5.5(b).

Figure 5.6 shows the effect of reloading/strain rate change on the compression stress-strain curves of all Al foams tested. It is depicted in the same figure that, although Alulight foam show no strain rate dependent compression stress, prepared Al foams compression stresses increase with increasing strain rate. It is concluded that Alulight foam behave as Type I, while prepared foams behave as Type II structure.

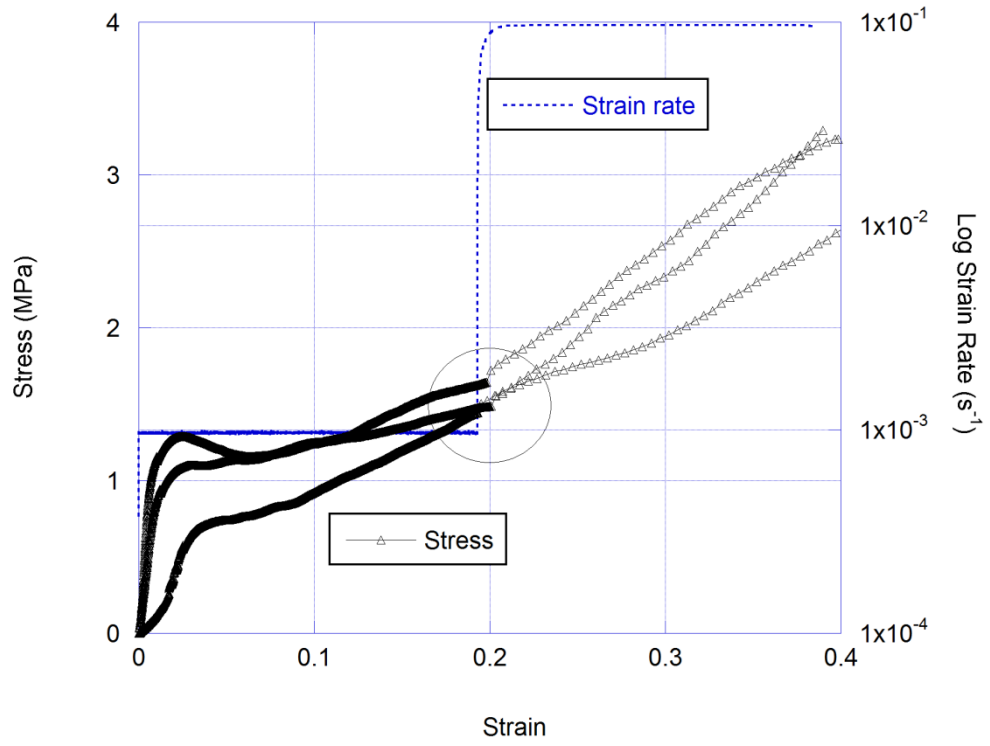


(a)

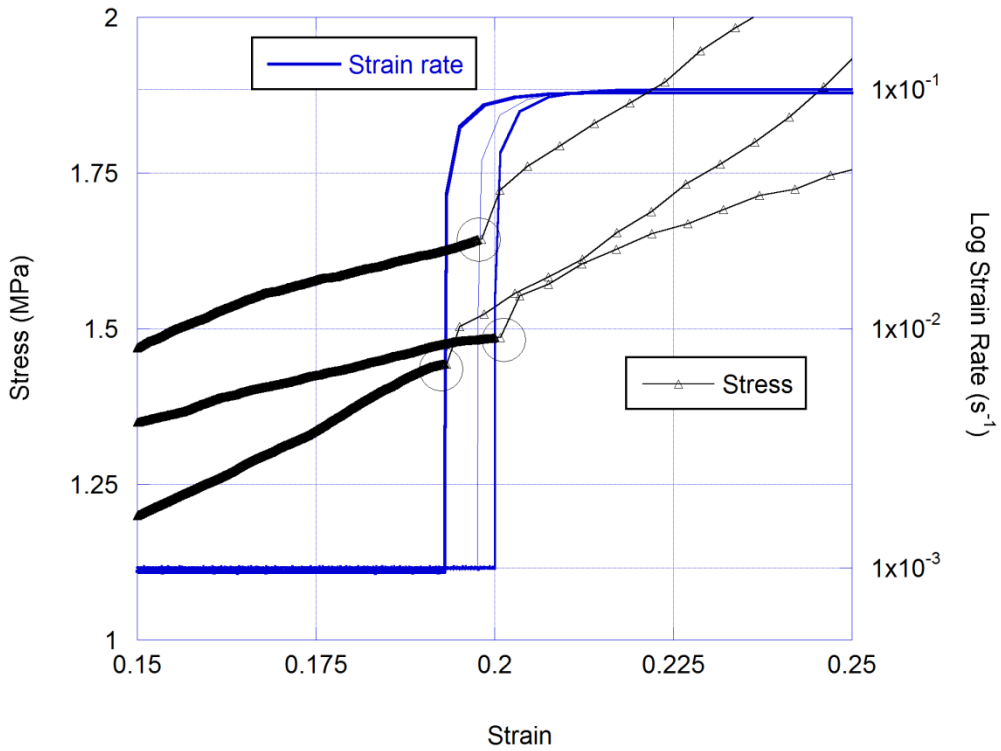


(b)

Figure 5.3. (a) Reloading compression stress-strain curves of tests of Al foams and (b) magnified reload curve .

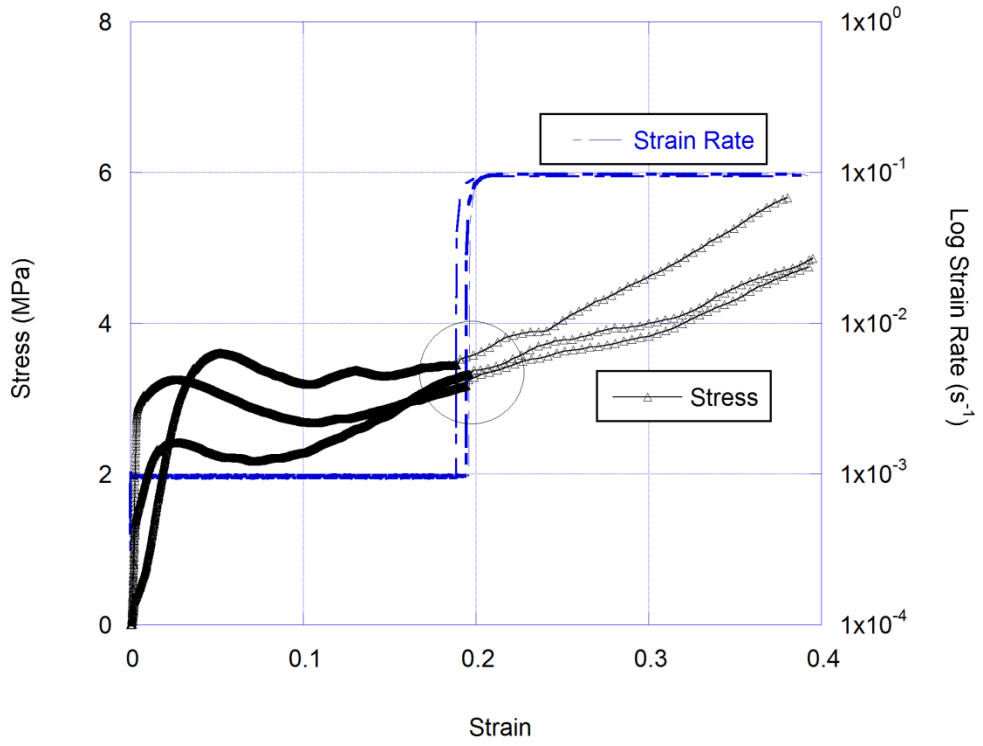


(a)

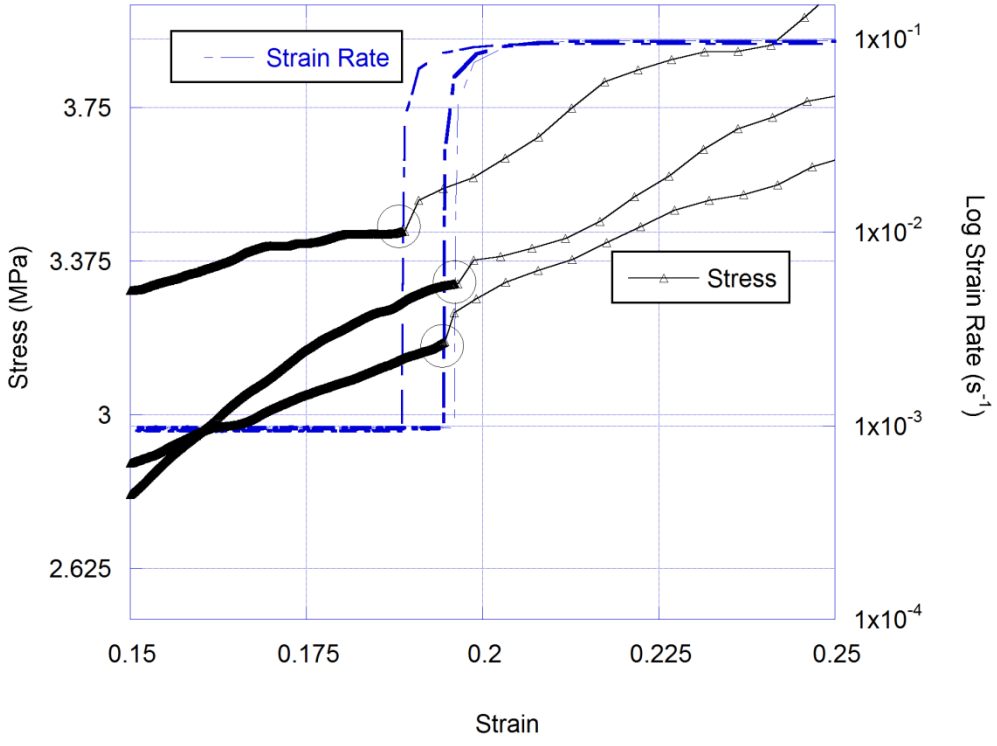


(b)

Figure 5.4. (a) Reloading compression stress-strain curves of tests of Al/SiC foams and (b) magnified reload curve.

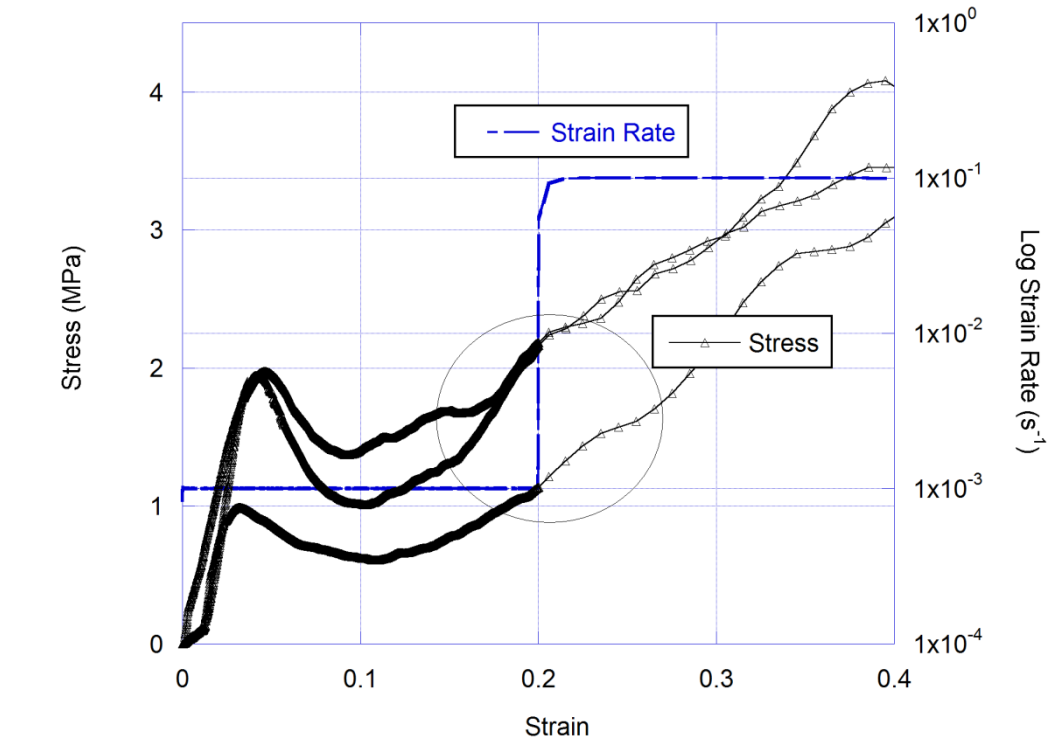


(a)

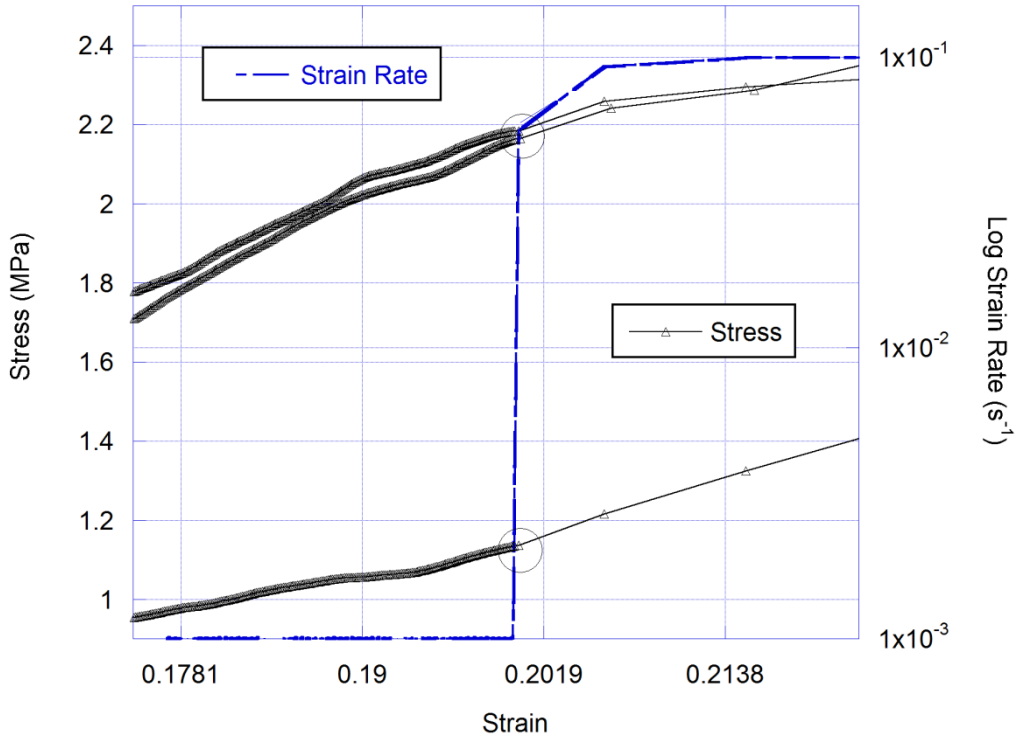


(b)

Figure 5.5. (a) Reloading compression stress-strain curves of tests of Alulight foams and (b) magnified reload curve.

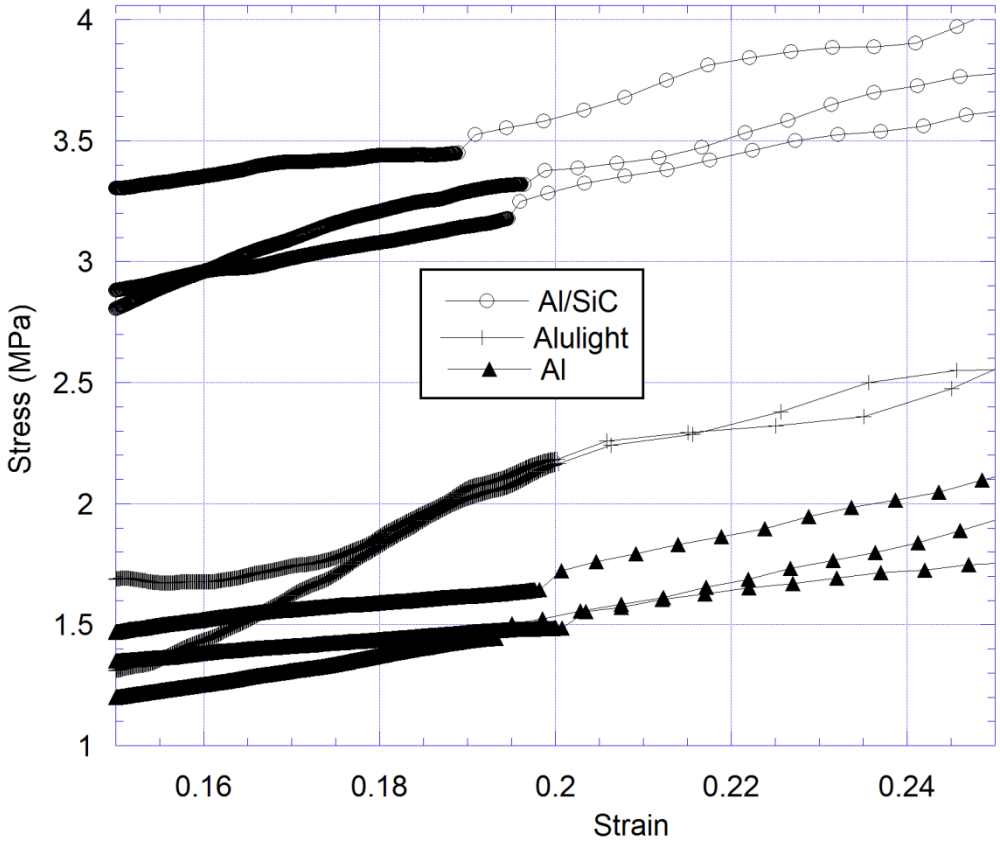


Figure 5.6. Comparison of stress strain curves of Alulight, Al and Al/SiC foams.

The deformed cross-section of a compression tested and recovered Al foam is shown in Figure 5.7(a). The deformation is seen in the same figure is a localized at the bottom section of the sample and the deformation proceeds from bottom to the upper sections (progressive). In the localized deformed region, the cell wall bending is clearly seen in Figures 5.7(b-c). The cell edges crush over the bent thin cell walls. Optical microscope pictures seen in Figures 5.7(b-d) show no fracture or cracking of the cell walls. SEM microscopic analysis further shows a ductile deformation of Al foam cells; the cell walls bends on the relatively thick cell edges (Figures 5.8 a and b). The bending is observed to start at relative thin section of the cell walls. Similar deformation behaviors are also observed in Al/SiC foams. The main deformation mechanism is the cell wall progressive cell wall bending as seen in Figures 5.9(a) and (b). Different from Al foams, few cell wall cracks near the cell edges are seen in Al/SiC foams (Figure 5.9 c and d). Since progressive bending occurs on the cell walls, strength enhancement in Al and Al/SiC foams is concluded to occur due to the micro-inertial effect.

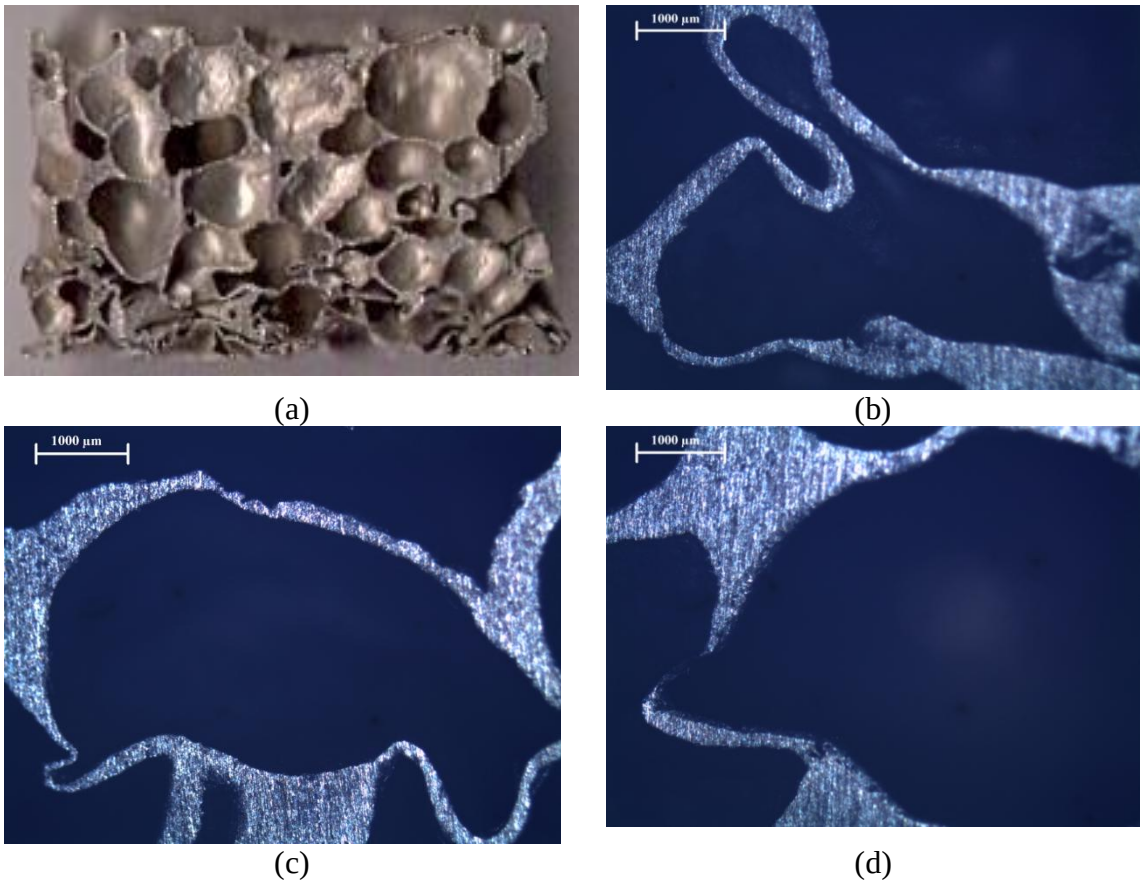


(a) (b)

(c) (d)

Figure 5.7. (a) Deformed cross-section and optical microscope pictures of the mounted deformed cross-section of Al foams; (b) bending on the cells walls and (c) and (d) cell wall bending on the cell edges.

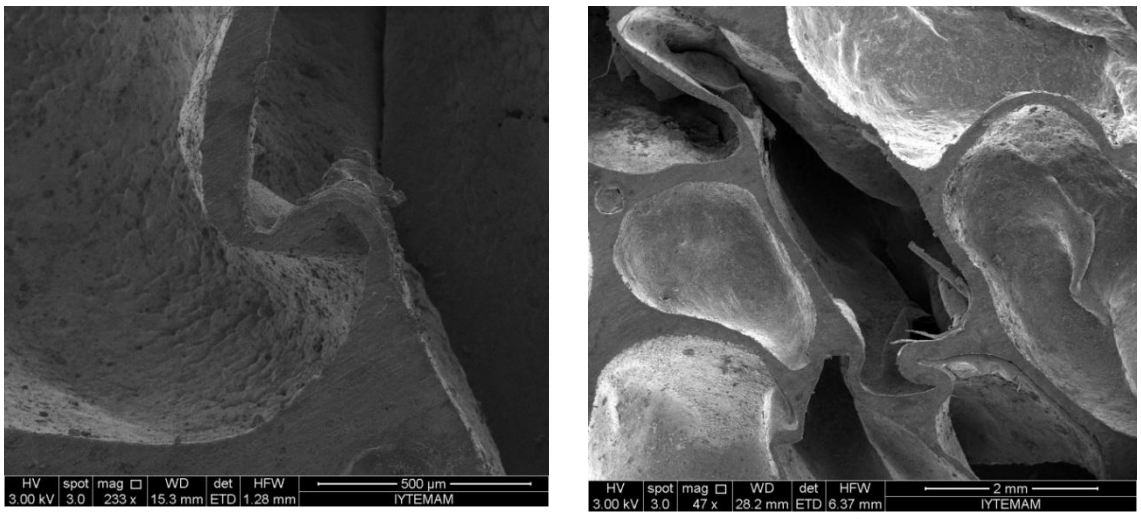


(a) (b)

Figure 5.8. SEM pictures deformed cross-sections of Al foam (a) cell wall bending and (b) cell wall bending on the cell edges.

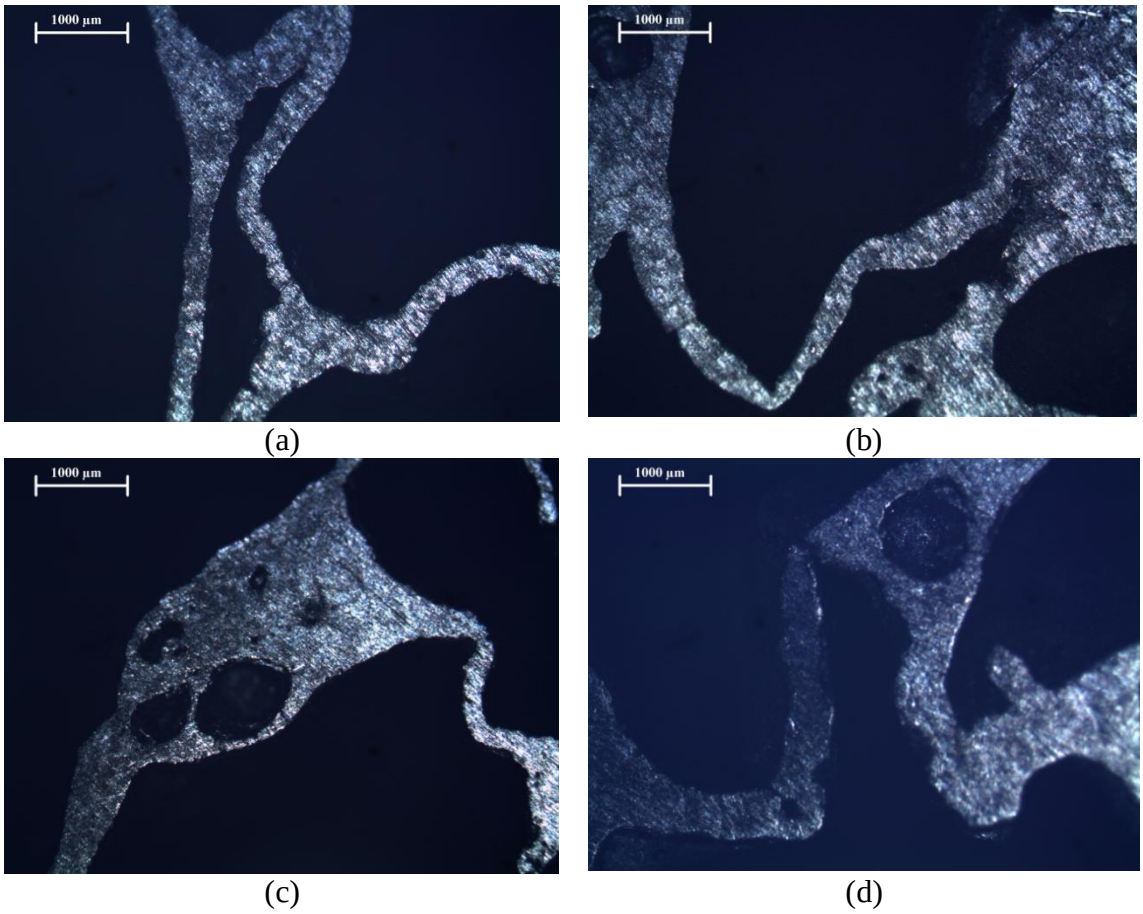


Figure 5.9. Optical microscope pictures of the mounted deformed cross-section of Al/SiC foams; (a) and (b) bending of the cells walls and (c) and (d) cell wall bending on the cell edges and cell wall fracture.

The deformed cross section of tested and recovered Alulight foam is shown in Figure 5.10(a). The deformation is seen in the same figure is localized, similar to prepared Al foams. In the localized deformation region, the cell wall deformation is observed to be dominated by the fracture/cracking of the cell walls (Figures 5.10 b-d). The fracture is observed to occur near the cell edges as depicted in Figures 11(a) and (b). This confirms the brittle nature of the tested Alulight foams. Since progressive cell wall fracture is dominant, the compression stress of Alulight foam is found to be insensitive to the micro-inertial effect.

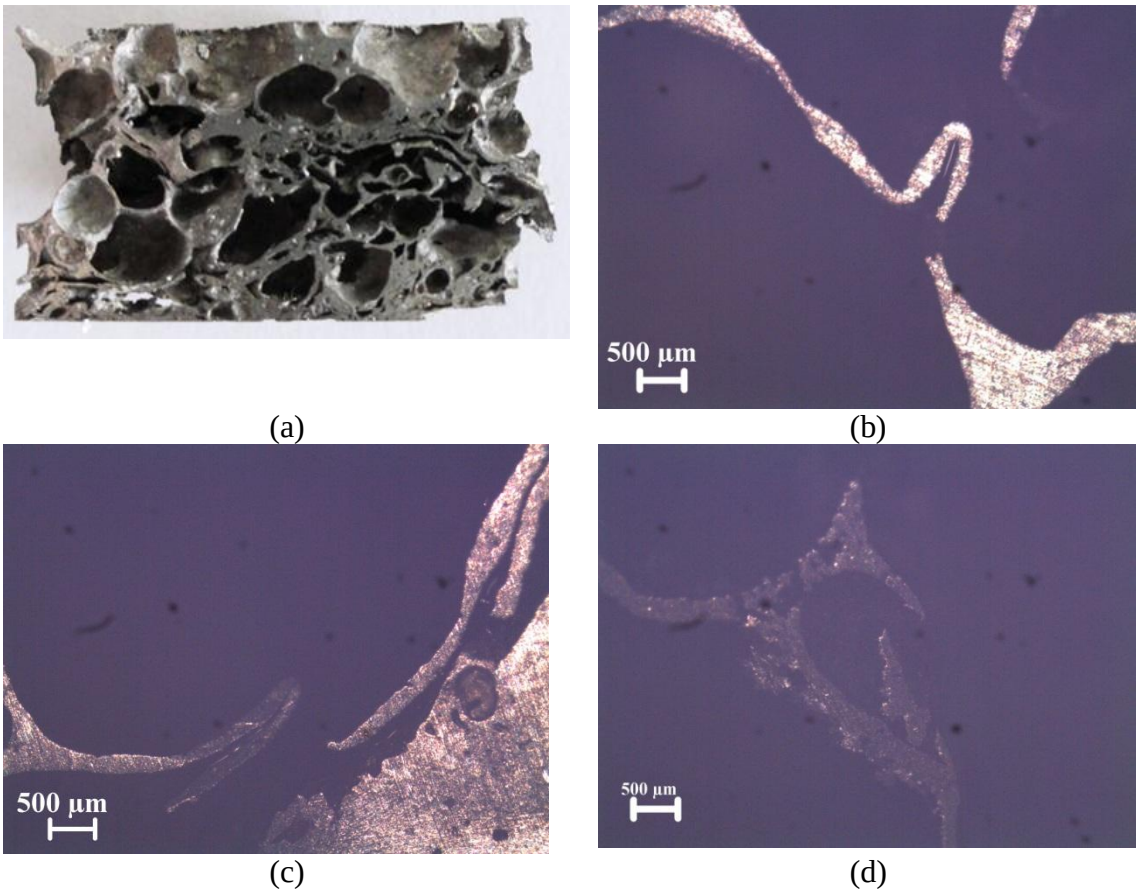


(a) (b)

(c) (d)

Figure 5.10. (a) deformed cross-section and optical microscope pictures of the mounted deformed cross-section of Alulight foams; (b) bending of the cells walls and cell wall fracture (c) and (d) cell wall fracture.

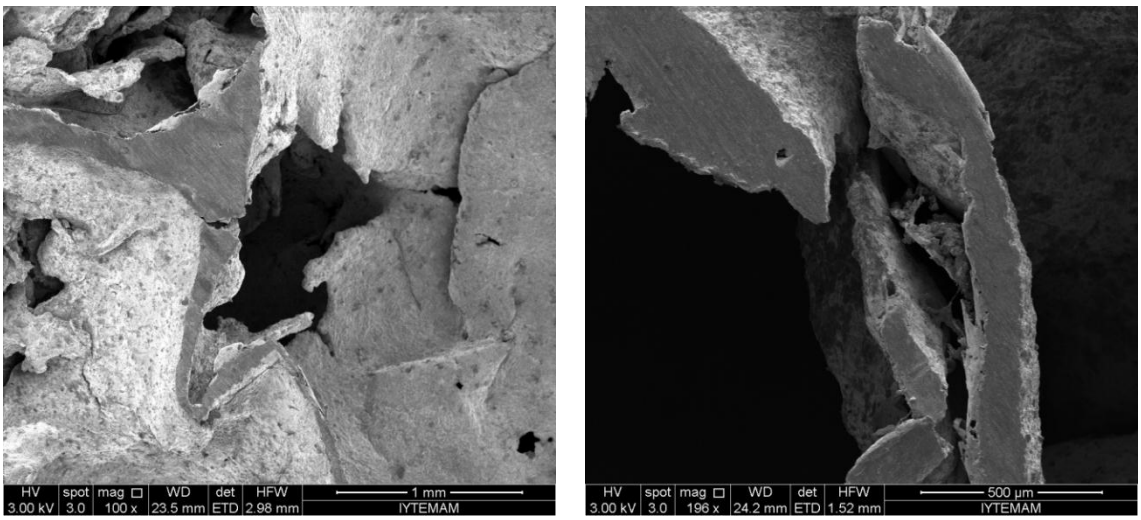


(a) (b)

Figure 5.11. SEM pictures deformed cross-sections of Alulight foam (a) cell wall fracture near cell edge and (b) cell wall fracture.

## 5.3. Quasi-static and Reloading Tests of Al Sandwich Plates

The compression stress-strain graphs of 20 mm thick $0^o/0^o$ oriented Al sandwich plates at $1x10^{-3}s^{-1}$ and $1x10^{-1}$ $s^{-1}$ are shown in Figure 5.12(a). The deformed picture of the tested plate until about 0.4 strains is also shown in the figure. The deformation, as seen in Figure 5.12(a), proceeds with the shearing of the fins at the brazing locations and partly with the bending of the fins. It is also noted in the same figure that the change in the deformation mode leads to two different stress-strain curves. When the deformation proceeds with the shearing of the fins between plates at the brazing points, the stress values following a peak stress decreases gradually. The peak stress is the point where the shear deformation starts. It is noted that when the deformation partly involves bending of the fins, the stress values increases following the initial reduction of the stress. These two behaviors are seen in Figure 5.12(a); the test at $1x10^{-1}$ $s^{-1}$ shows former and the test at $1x10^{-3}$ $s^{-1}$ shows the later behavior. Because of change in deformation mode, the determination of strain rate dependent deformation behavior of the tested plate is rather difficult.

In Figures 5.12(b) and (c), the reloading stress-strain curves of tested Al plate are shown. The tested plate shows stress reductions following the initial peak stress, showing aforementioned former stress-strain behavior (Figure 5.12b). It is also noted in Figure 5.12(c) that increasing strain rate from $1x10^{-3}s^{-1}$ to $1x10^{-1}$ $s^{-1}$ has almost no effect on the stress values, showing Type I deformation behavior. This behavior is in accord with the deformation characteristics of the tested Al plate as the fins are sheared between the Al plates, leading to very little bending of the fins. Therefore, it is concluded that 20 mm thick $0^o/0^o$ oriented Al sandwich plates show inertia insensitive deformation behavior.

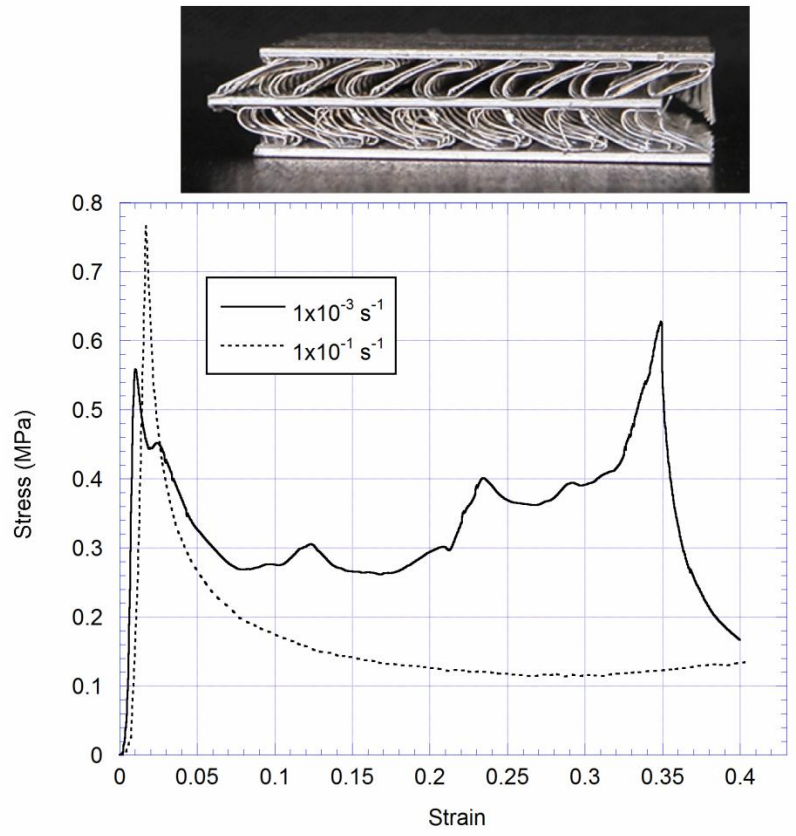


(a)

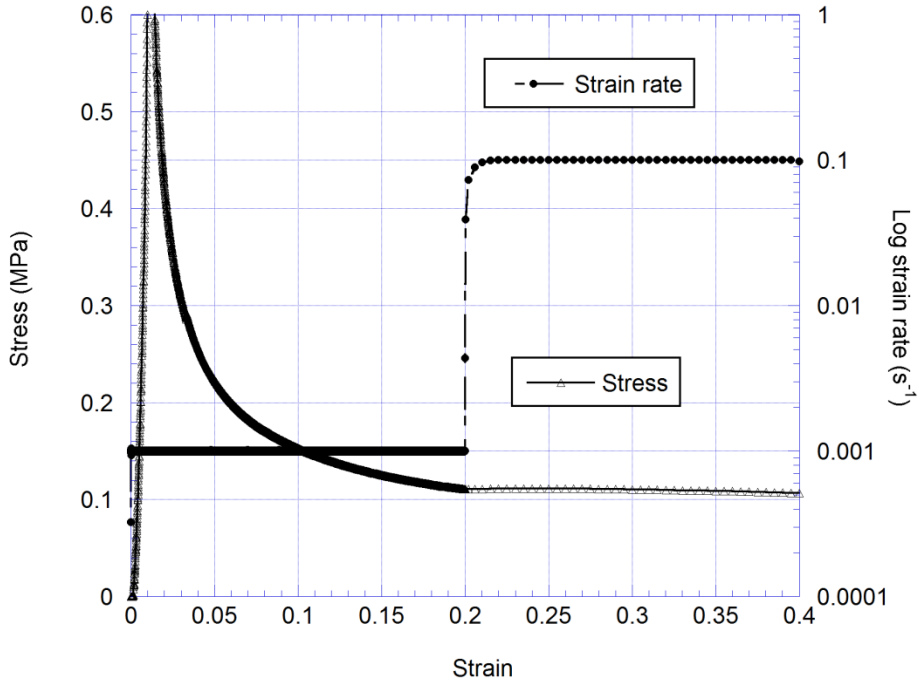


(b)

Figure 5.12. Stress-strain behavior of 20 mm thick $0^o/0^o$ oriented Al sandwich plates; (a) at $1x10^{-3}s^{-1}$ and $1x10^{-1}$ $s^{-1}$ and (b) and (c) reloading test.

**(cont. on next page)**

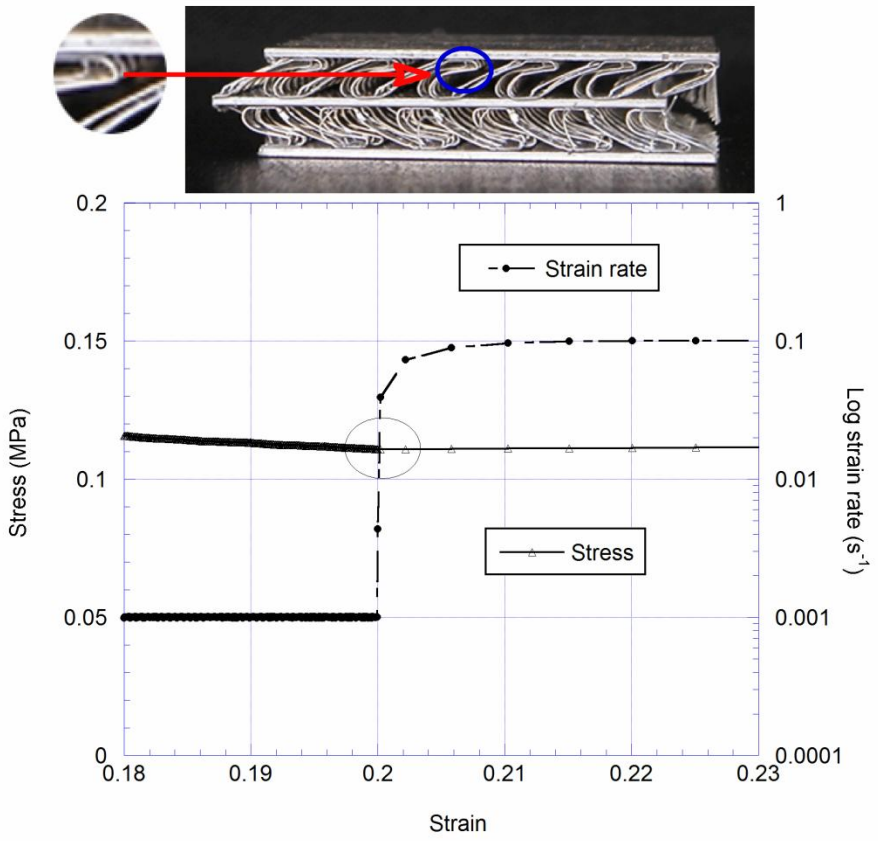


(c)

Figure 5.12. (cont.)

The compression stress-strain graphs of 20 mm thick $0^o/90^o$ oriented Al sandwich plates at $1x10^{-3}$ $s^{-1}$ and $1x10^{-1}$ $s^{-1}$ are shown in Figure 5.13(a). The deformed picture of the tested plate until about 0.4 strains is also shown in the figure. The deformation is, as seen in Figure 5.13(a), progressive bending of the fin layers; first layer bends followed by the bending of the second layer. Following the initial peak stress, corresponding to the start of collapse of the first fin layer, the stress values fluctuate around a plateau stress value. Furthermore, the tested Al plate is noted to show a strain rate dependent plateau stress (Figure 5.13a): as the strain rate increases the compression stress values increases in the plateau region. In Figures 5.13(b) and (c), the reloading stress-strain curve of tested Al plate is shown. In accord with tests at different strain rates, increasing strain rate from $1x10^{-3}$ $s^{-1}$ to $1x10^{-1}$ $s^{-1}$ in reloading test increases the stress values as seen in Figure 5.13(c). This behavior, inertia sensitive compression stress values, is well accord with Type II deformation behavior.

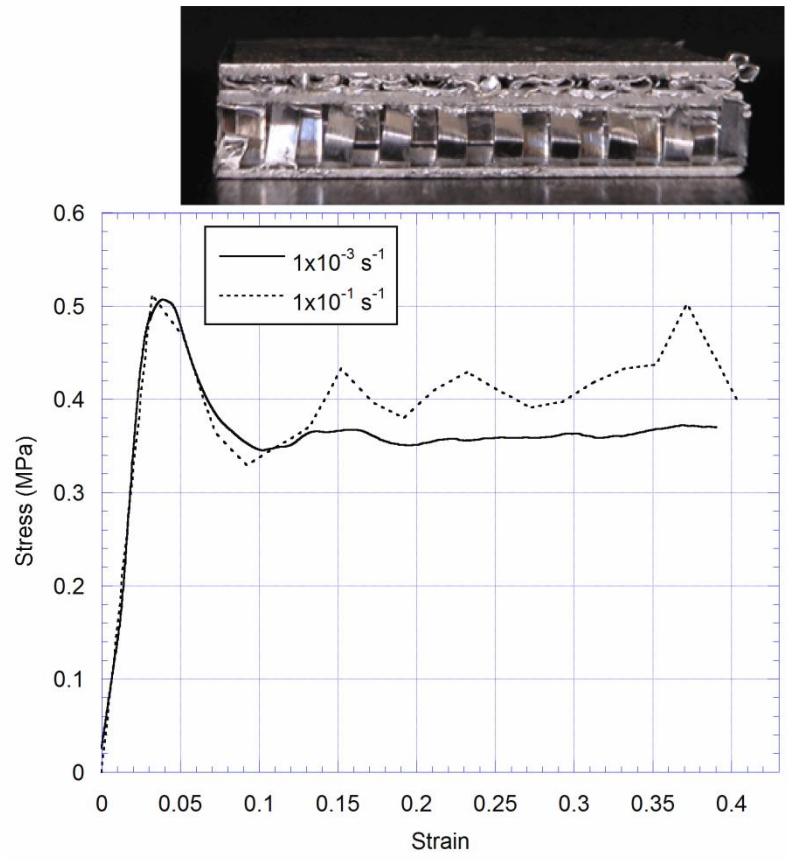


(a)

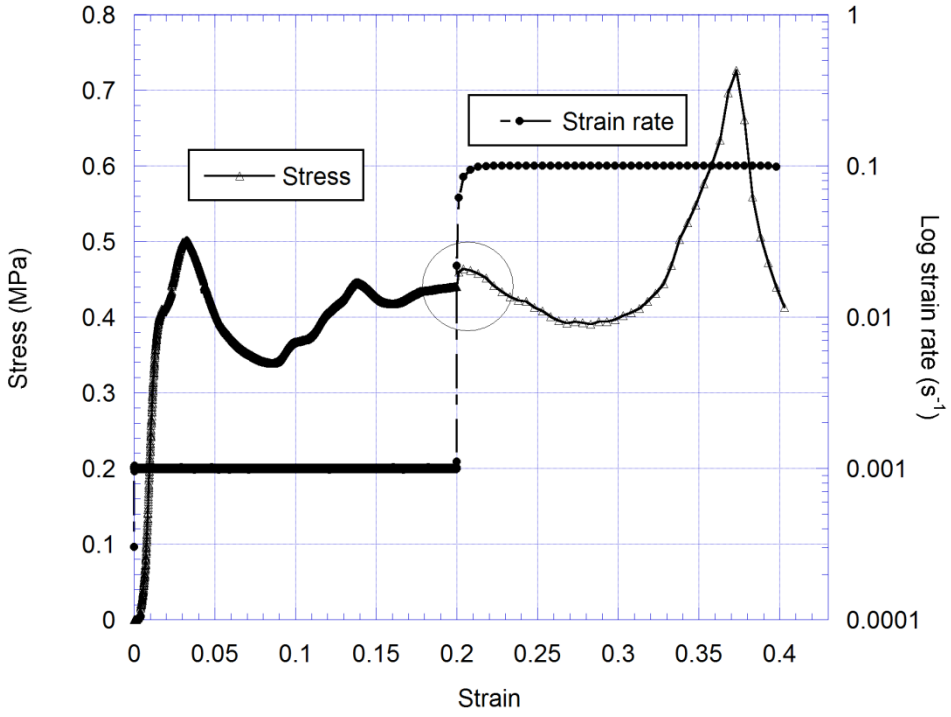


(b)

Figure 5.13. Stress-strain behavior of 20 mm thick $0^o/90^o$ oriented Al sandwich plate; (a) at $1x10^{-3}$ $s^{-1}$ and $1x10^{-1}$ $s^{-1}$ and (b) and (c) reloading test.

**(cont. on next page)**

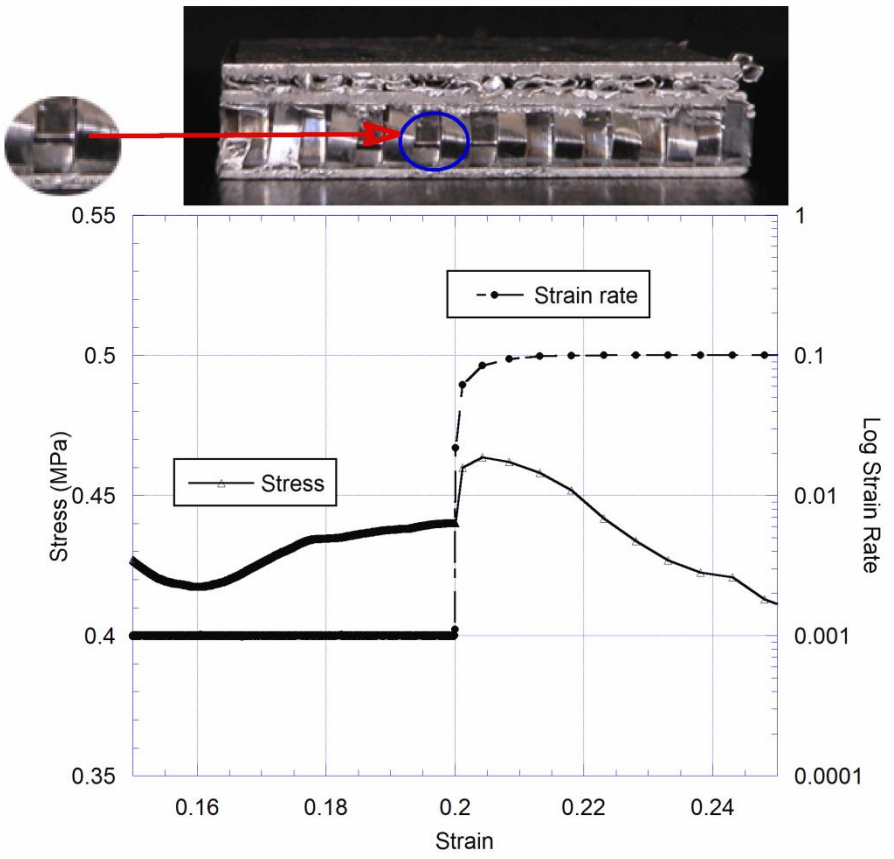


(c)

Figure 5.13. (cont.)

The compression stress-strain and reloading curves of 28 mm thick $0^o/0^o$ oriented Al sandwich plates are shown in Figure 5.14(a). The deformed picture of the tested plate until about 0.4 strains is also shown in the same figure. Similar to 20 mm thick $0^o/0^o$ oriented Al sandwich plates, the deformation proceeds with the shearing of the Al plates except the initial deformation region of the stress strain curve. In the initial region, fins are observed to bend until about 0.1 strains; thereafter, Al plates are sheared and stress values decrease. Although, in the initial region, the deformation is seen to be strain rate dependent, in the following stress reduction region no strain rate sensitivity is seen in the stress values (Figure 5.14a). The reloading test in the stress reduction region also shows that increasing strain rate from $1x10^{-3}$ $s^{-1}$ to $1x10^{-1}$ $s^{-1}$ has almost no effect on the stress values as seen in Figure 5.14(b). Therefore, it is concluded that 28 mm thick $0^o/0^o$ oriented Al sandwich plates show inertia insensitive deformation behavior.

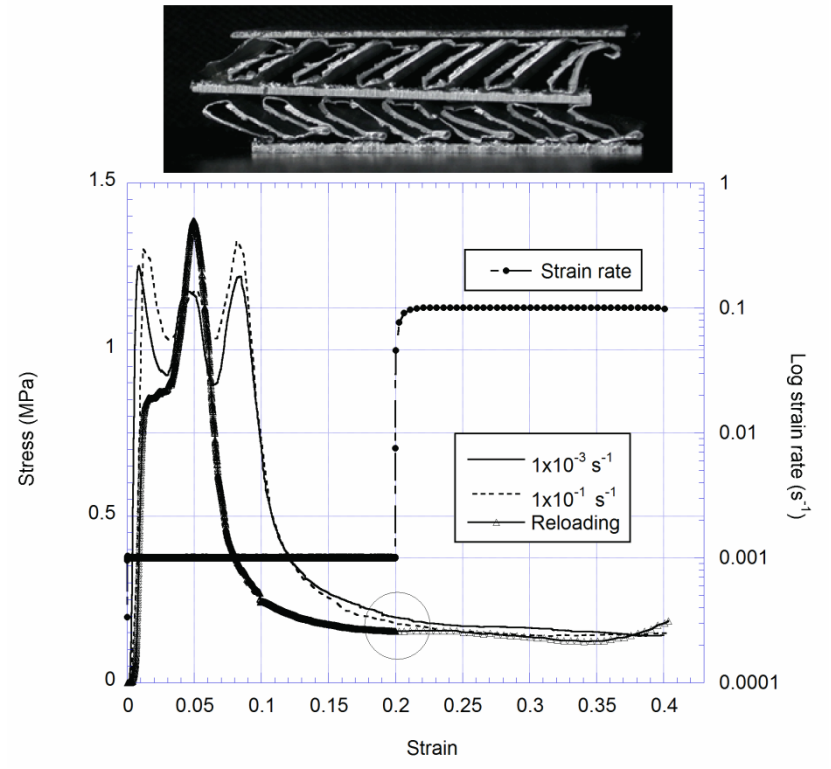


(a)

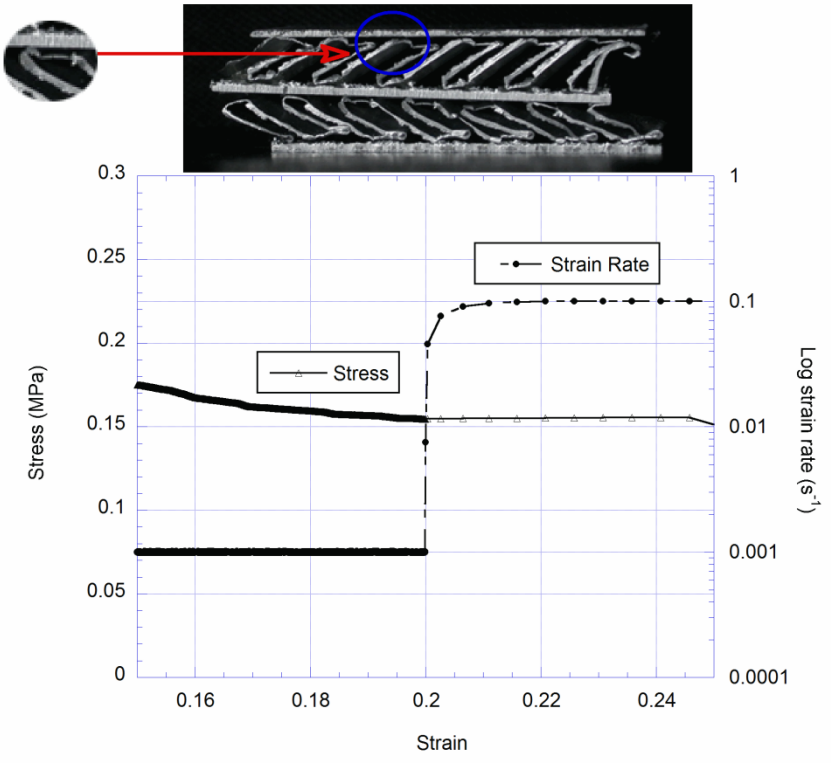


(b)

Figure 5.14. (a) Stress-strain behavior of 28 mm thick $0^o/0^o$ oriented Al sandwich plates and (b) reloading test.

The compression stress-strain and reloading graphs of 28 mm thick $0^o/90^o$ oriented Al sandwich plates are shown in Figure 5.15(a). The deformed picture of the tested plate until about 0.4 strains is also shown in the figure. The deformation is observed to proceeds with progressive bending at the beginning of the deformation then followed by irregular bending of the fins. As the fins are bent irregularly, the reloading test shows a less dependence on inertia (Figure 5.15b). It is concluded that 28 mm thick $0^o/90^o$ oriented Al sandwich plates show a deformation behavior between Type I and Type II structures.

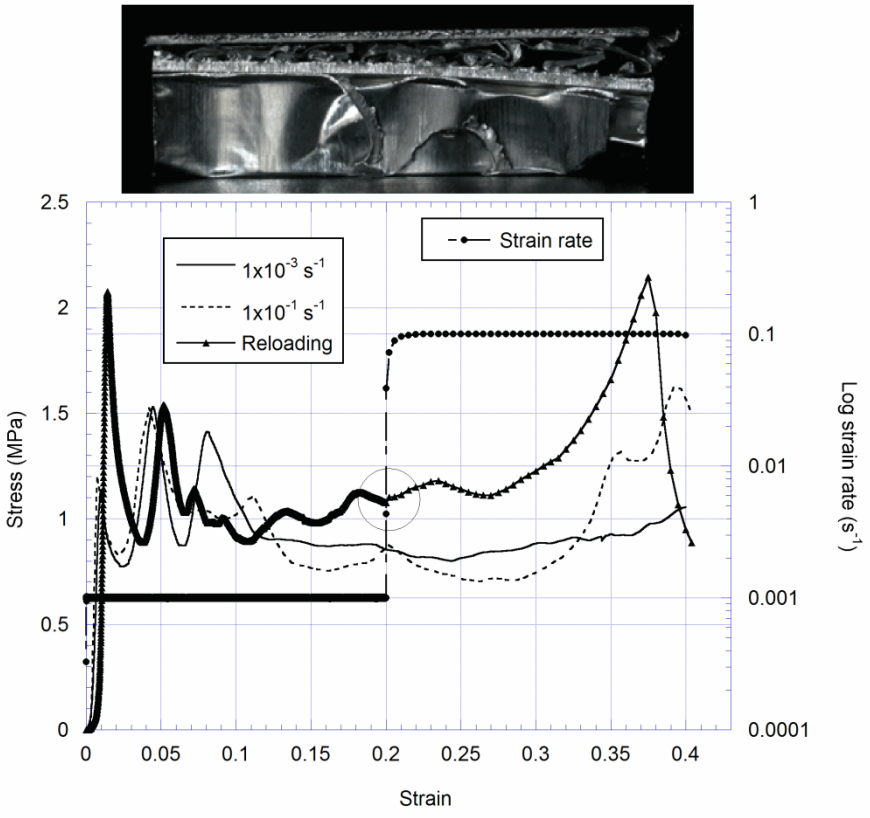


(a)

Figure 5.15. (a) Stress-strain behavior of 28 mm thick $0^o/90^o$ oriented Al sandwich plates and (b) reloading test.

**(cont. on next page)**

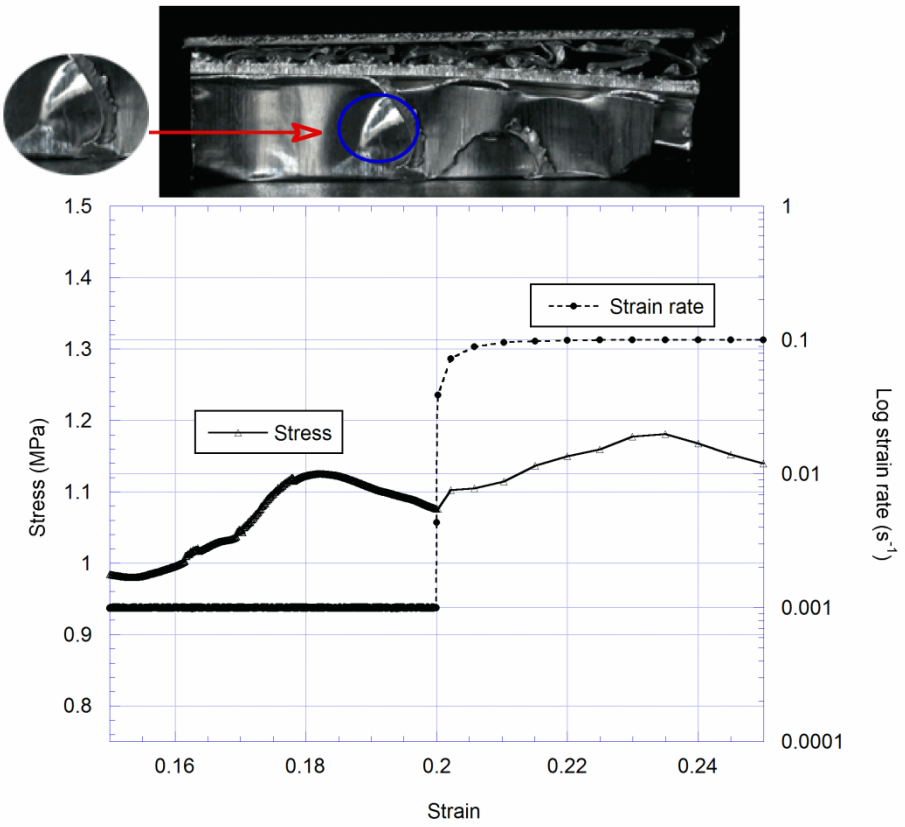


(b)

Figure 5.15. (cont.)

The compression and reloading stress-strain graphs of 42.5 mm thick $0^o/90^o$ oriented Al sandwich plates at $1x10^{-3}$ $s^{-1}$ and $1x10^{-1}$ $s^{-1}$ and are shown in Figure 5.16(a). The deformed picture of the tested plate until about 0.4 strains is also shown in the figure. The deformation is, as seen in Figure 5.16(a), progressive bending of the fin layers. The tested Al plate is also noted to show a strain rate dependent plateau stress (Figure 5.16a); as the strain rate increases the compression stress values increases in the plateau region. The reloading stress-strain curve of tested Al plate shows also inertia sensitive compression stress values, well accord with Type II deformation behavior (Figure 5.16b).

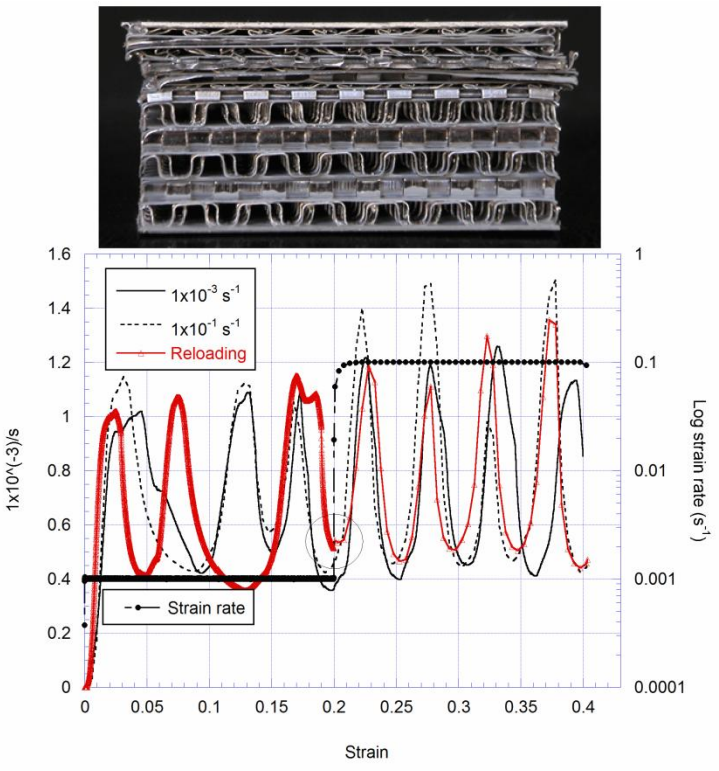


(a)

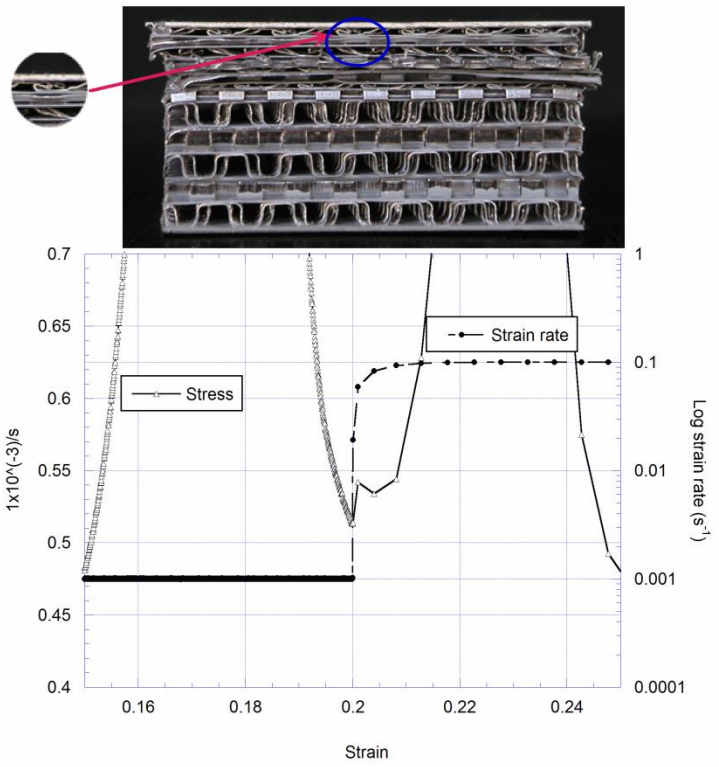


(b)

Figure 5.16. (a) Stress-strain behavior of 42.5 mm thick $0^o/90^o$ oriented Al sandwich plates and (b) reloading test.

## 5.4. Quasi-static and Reloading Tests of Glass Foams

The reloading compression stress-strain curves of glass foam samples are shown in Figure 5.17(a). The curves show typical characteristics of the brittle cellular solids; the foam cells crush progressively under compressive loads and result in fluctuating stresses as depicted in Figure 5.17(a). Reloading tests result in almost no effect on the stress values (Figure 5.17b). The samples tested are therefore inertia insensitive as it is expected.

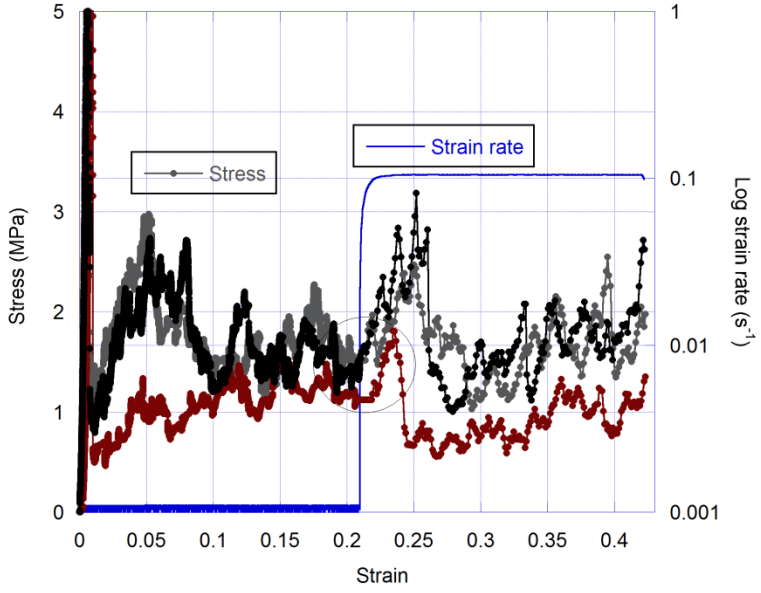


(a)

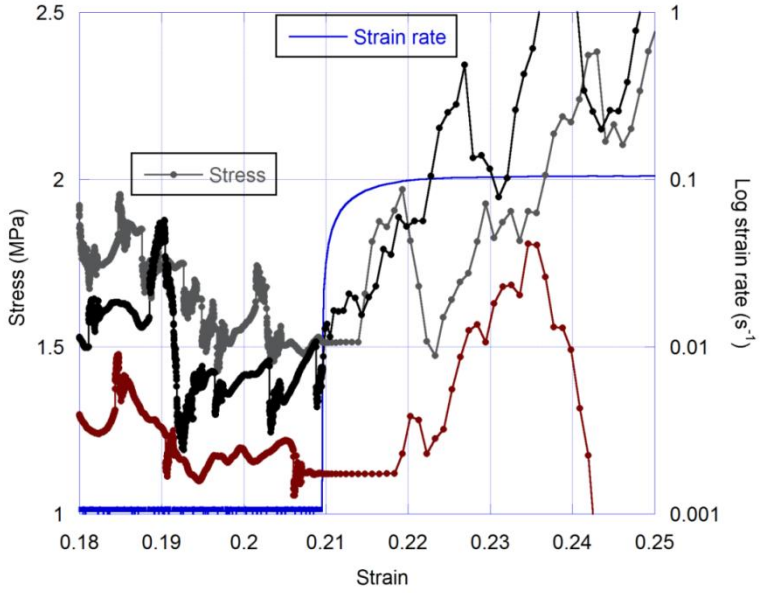


(b)

Figure 5.17. Reloading tests on glass foams (a) stress-strain curve and (b) magnified stress-strain curve.

## 5.5. High Strain Rate Tests of Al Foams

Typical incident, reflected and transmitted waves in SHPB Al foam testing are shown in Figure 5.18 as function of time. Quasi-static and SHPB high strain rate stress-strain and strain rate-strain curves of Al foams of two different foam densities are shown in Figure 5.19. SHPB high strain rate test were performed at about 400 $s^{-1}$. Increasing strain rate from $1x10^{-3}$ $s^{-1}$ at quasi-static strain rates to 400 $s^{-1}$ at high strain rates in SHPB, increases the foam plateau stress from 0.5 to 1 MPa and from 1.5 to 2 MPa depending on the density of the foam tested. These prove an inertia effect on the foam plateau stress, a result confirming the reloading tests. Quasi-static and SHPB high strain rate stress-strain and strain rate-strain curves of Al/SiC foams of two different foam densities are shown in Figure 5.20. SHPB high strain rate test were performed at about 400 $s^{-1}$. Increasing strain rate from $1x10^{-3}$ $s^{-1}$ at quasi-static strain rates to 400 $s^{-1}$ at high strain rates in SHPB, increases the foam plateau stress from 1.5 to 2 MPa and from 4 to 4.8 MPa depending on the density of the foam tested. Similar to reloading tests, SHPB test results confirm the inertia effect on Al/SiC foams. Quasi-static and SHPB high strain rate stress-strain and strain rate-strain curves of Al foams of two different foam densities are shown in Figure 5.21. SHPB high strain rate test were performed at about 400 $s^{-1}$. As seen in Figure 5.21, SHPB tests have no effect on Alulight foam plateau stress, showing inertia independent foam plateau stresses.

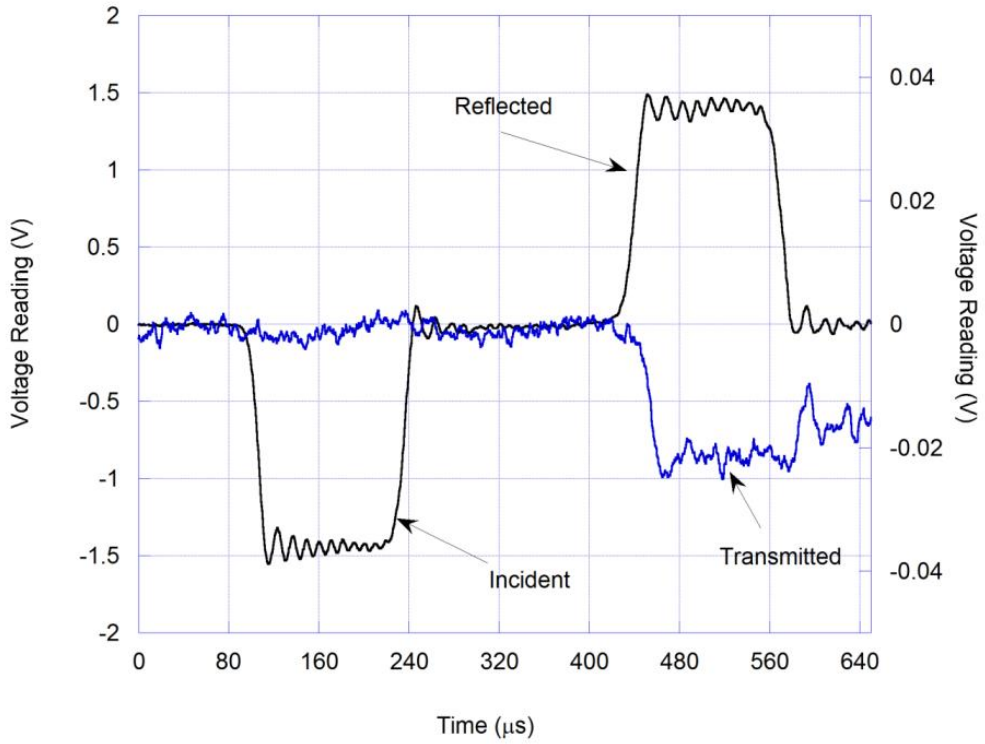


Figure 5.18. Typical stress waves in SHPB Al foam testing.

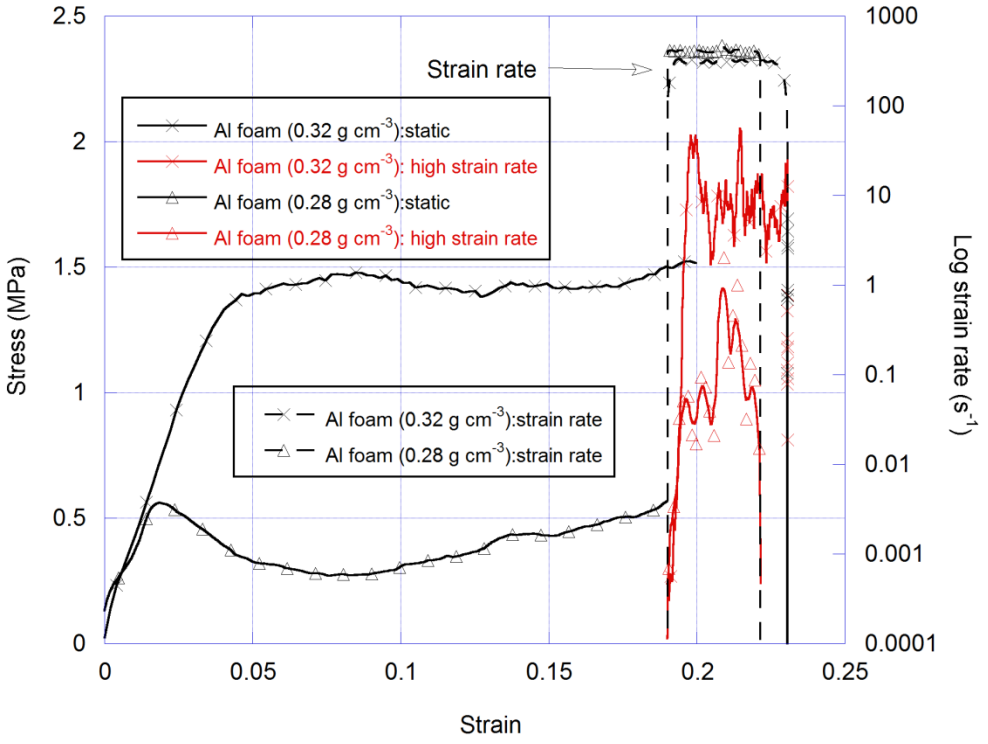


Figure 5.19. Quasi-static and SHPB compression tests of Al foams.

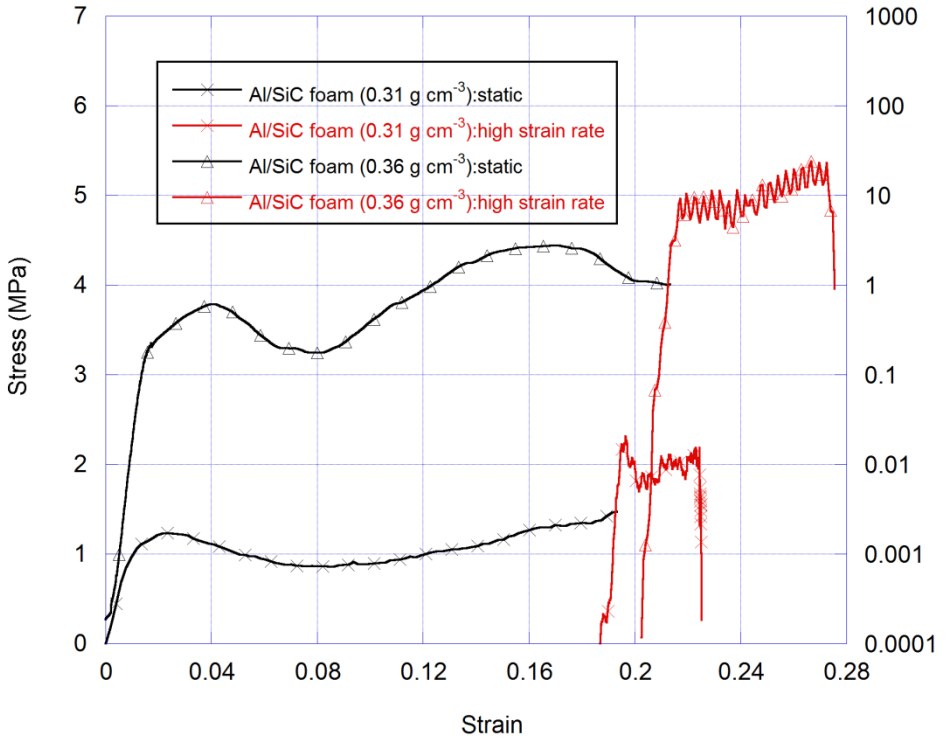


Figure 5.20. Quasi-static and SHPB compression tests of Al/SiC foams.

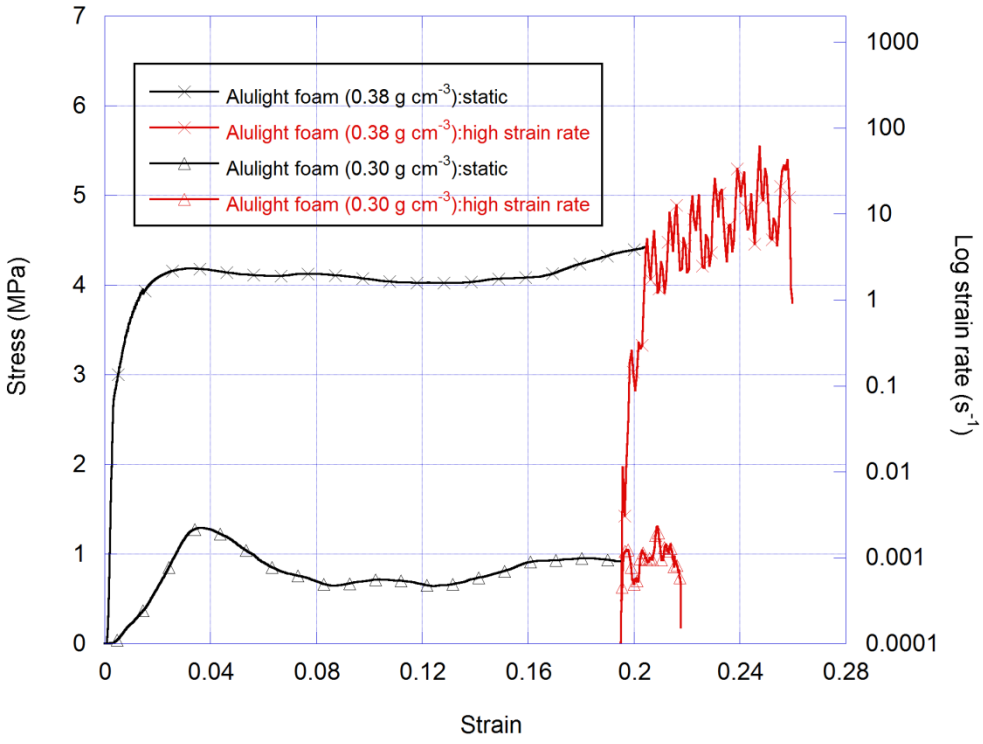


Figure 5.21. Quasi-static and SHPB compression tests of Alulight foams.

## 5.6. Analysis of Experimental Results

The load-displacement and displacement rate-displacement curves of the reloaded Al extruded tubes through lateral and axial directions clearly show two different responses to inertial forces. Tube lateral deformation is found to be not effected from micro-inertia, reflecting Type I behavior (Calladine and English 1984). Tube axial deformation proceeded by progressive bending of tube wall shows inertia sensitive deformation, reflecting Type II deformation behavior (Calladine and English 1984).

As stated earlier, the strain rate sensitive crushing stresses of cellular materials may results from the strain rate sensitivity of the cell wall, the micro-inertial effects, shock wave propagation and the compressed air pressure in the cells (Zhao, et al. 2005). The effect compressed air pressure in dynamic loading and shock wave propagation within the strain rate regime of the SHPB testing was previously shown to be insignificant (Deshpande and Fleck 2000, Reid and Peng 1997). It should also be noted that Al and its alloys have known to have strain rate independent flow stress (Deshpande and Fleck 2000, Hall, et al. 2000, Kenny 1996, Smerd, et al. 2005, Wu and Jiang 1997, Zhao and Gary 1998). Therefore, micro inertia is assumed to be only responsible for the increased deformation stresses in Al tubes, Al foams and Al sandwich plates tested in this thesis.

The lack of strain rate sensitivity of the tested Alulight foam produced through powder route within the studied strain rate regime is well accord with the results of the previous high strain rate tests performed on the similar foams produced by the same route (Deshpande and Fleck 2000, Hall, et al. 2000, Peroni, et al. 2008). Microscopic studies have clearly shows that the foam cell walls fracture just before and after bending of the cell edges on the cell walls. While, the Al foams with ductile cellular structure such as Alporas foams show strain rate sensitive deformation or plateau stresses as stated earlier (Miyoshi, et al. 2000, Mukai, et al. 1999, Mukai, et al. 2006, Paul and Ramamurty 2000). Al foams with and without SiC addition show very similar response to strain rate simply arising from relatively more ductile cell structures. This is also proved by the microscopic observations. It should be noted that depending on SiC particulate weight percent and the material from which foam made, the observed strain rate sensitivity is demolished due to the micro cracking of the cell walls as previously

shown for Cymat Al foams (Kenny 1996). It is clear that inertia effect involved in successive folding is the main cause for the strength enhancement of both Al foams and sandwich plates. Above findings were also proved with the SHPB compression tests in which strain rate effect on the plateau stress was only found in Al and Al/SiC foams, while Alulight foams deformed dynamically at the similar stress levels with quasi-static strain rates.

This study also shows that the layer configuration/orientation may affect the micro inertia effect on deformation of Al sandwich plates. 20 mm thick Al sandwich plates experience different crushing stresses and deformation modes depending on the layer orientations. The stresses are higher for $0^o/90^o$ orientation than for $0^o/0^o$ orientation. The deformation mode is bending of the fins in $0^o/90^o$ orientation while, in $0^o/0^o$ orientation it shearing of face sheets on fins. These deformation modes result in micro inertia deformation mode in $0^o/90^o$ orientation and micro inertia insensitive deformation mode in $0^o/0^o$ orientation. Two 8.5 mm thick Al fin plates combined together in $0^o/0^o$ orientation and 1mm thick of Al sheets were used between the layers and as face sheets (Figures 4.10(a) and (b)). A similar effect of layer orientation is also found for 28 mm thick Al sandwich plates. In the designing Al sandwich plates with corrugated interlayers, on should consider the layer orientation in order to assess both crushing stresses and micro inertia effect.

The strain rate independent crushing behavior of the tested glass foams within the studied strain rate regime also confirms the effect of deformation mode on the micro inertia effect. Simply, brittle fracture of the cells demolishes the micro inertia effect.

Above all, a simple testing method was shown in this thesis to investigate micro inertia effect in hollow and cellular Al structures. This simple method is dependent on quasi-static testing of the structures through reloading from a lower strain rate to a higher strain rate.

# CHAPTER 6

# CONCLUSIONS

In this thesis Al tubes, Al foams of different types, Al sandwich plates of various configurations and brittle glass foam samples were quasi-statically reloaded in order to assess any micro inertia effect on the deformation stresses. Al foams tested quasi-statically were further reloaded (interrupted test) in SHPB at dynamic strain rates in order to see effect of strain rate on micro inertia effect. Followings were concluded;

1. Al empty tubes showed characteristic Type I behavior in lateral compression and Type II behavior in axial compression.
2. The lack of strain rate sensitivity of the tested Alulight foam produced through powder route within the studied strain rate regime was due to the foam cell wall fracture. While Al foams with and without SiC addition showed micro inertia effect through progressive cell wall bending.
3. Al and Al/SiC foams showed the strain rate sensitive plateau stress in the SHPB compression tests, while Alulight foams showed no strain rate sensitivity. These results were in accord with reloading tests at quasi-static strain rates.
4. The layer configuration/orientation affected the micro inertia effect in Al sandwich plates. Progressive bending of the interlayer fins resulted in strain rate depending crushing stress, while shearing of the interlayer resulted in strain rate insensitive deformation stress.
5. As was expected, the strength enhancement was not seen in glass foam specimens tested as the cell walls were fractured under compressive loads.
6. A simple testing method was shown to investigate micro inertia effect in hollow and cellular Al structures.

# REFERENCES


Ashby, M. F., Evans, A. G., Fleck, N. A., Gibson, L. J., Hutchinson, J. W. and Wadley, H. N. G., 2000, Making metal foams, Metal Foams ed. 6-23, Butterworth-Heinemann.

Banhart, J., 2005, Aluminium foams for lighter vehicles. *International Journal of Vehicle Design*. 37(2-3): p. 114-125.

Banhart, J., Baumeister, J. and Weber, M., 1996, Damping properties of aluminium foams. *Materials Science and Engineering A*. 205(1-2): p. 221-228.

Baumeister, J. and Schrader, H., 1992, US Patent No.5151246, 5151246.

Baumgärtner, F., Duarte, I. and Banhart, J., 2000, Industrialization of Powder Compact Toaming Process. *Advanced Engineering Materials*. 2(4): p. 168-174.

Beals, J. T. and Thompson, M. S., 1997, Density gradient effects on aluminium foam compression behaviour. *Journal of Materials Science*. 32(13): p. 3595-3600.

Calladine, C. R. and English, R. W., 1984, Strain-rate and inertia effects in the collapse of two types of energy-absorbing structure. *International Journal of Mechanical Sciences*. 26(11-12): p. 689-701.

Degischer, H. P., 2003, Strengths, Weaknesses, and Opportunities, Wiley-VCH Verlag GmbH & Co. KGaA.

Deshpande, V. S. and Fleck, N. A., 2000, High strain rate compressive behaviour of aluminium alloy foams. *International Journal of Impact Engineering*. 24(3): p. 277-298.

Fang, Dai-Ning, Li, Yu-Long and Zhao, Han, 2010, On the behaviour characterization of metallic cellular materials under impact loading. *Acta Mechanica Sinica*. 26(6): p. 837-846.

Gibson, L. J., 2000, Mechanical behavior of metallic foams. *Annual Review of Materials Science*. 30: p. 191-227.

Gibson, Lorna J., 1988, Cellular solids : structure & properties / Lorna J. Gibson, Michael F. Ashby, Pergamon Press.

Gibson, Lorna J. and Ashby, M. F., 1997, Cellular solids : structure and properties, Cambridge University Press.

Goldsmith, Werner and Sackman, Jerome L., 1992, An experimental study of energy absorption in impact on sandwich plates. *International Journal of Impact Engineering*. 12(2): p. 241-262.

Guden, M. and Yüksel, S., 2006, SiC-particulate aluminum composite foams produced from powder compacts: foaming and compression behavior. *Journal of Materials Science*. 41(13): p. 4075-4084.

Güden, M. and Kavi, H., 2006, Quasi-static axial compression behavior of constraint hexagonal and square-packed empty and aluminum foam-filled aluminum multi-tubes. *Thin-Walled Structures*. 44(7): p. 739-750.

Hall, I. W., Guden, M. and Yu, C. J., 2000, Crushing of aluminum closed cell foams: density and strain rate effects. *Scripta Materialia*. 43(6): p. 515-521.

Kathuria, Y. P., 2001, Laser assisted aluminum foaming. *Surface and Coatings Technology*. 142-144: p. 56-60.

Kenny, L.D., 1996, Mechanical Properties of Particle Stabilized Aluminum Foam. *Materials Science Forum*. 217 - 222(1883): p. 1883-1890.

Kitazono, K., Sato, E. and Kuribayashi, K., 2004, Novel manufacturing process of closed-cell aluminum foam by accumulative roll-bonding. *Scripta Materialia*. 50(4): p. 495-498.

Klintworth, J. W. and Stronge, W. J., 1988, Elasto-plastic yield limits and deformation laws for transversely crushed honeycombs. *International Journal of Mechanical Sciences*. 30(3-4): p. 273-292.

Langseth, M. and Hopperstad, O. S., 1996, Static and dynamic axial crushing of square thin-walled aluminium extrusions. *International Journal of Impact Engineering*. 18(7-8): p. 949-968.

Lankford, J. and Dannemann, KA, 1998, Strain rate effects in porous materials. *Proceedings of the Symposium of the Materials Research Society*. 521.

Lee, S., Barthelat, F., Hutchinson, J. W. and Espinosa, H. D., 2006, Dynamic failure of metallic pyramidal truss core materials - Experiments and modeling. *International Journal of Plasticity*. 22(11): p. 2118-2145.

Ma, G. W., Ye, Z. Q. and Shao, Z. S., 2009, Modeling loading rate effect on crushing stress of metallic cellular materials. *International Journal of Impact Engineering*. 36(6): p. 775-782.

Miyoshi, T., Itoh, M., Akiyama, S. and Kitahara, A., 2000, ALPORAS Aluminum Foam: Production Process, Properties, and Applications. *Advanced Engineering Materials*. 2(4): p. 179-183.

Mukai, T., Kanahashi, H., Miyoshi, T., Mabuchi, M., Nieh, T. G. and Higashi, K., 1999, Experimental study of energy absorption in a close-celled aluminum foam under dynamic loading. *Scripta Materialia*. 40(8): p. 921-927.

Mukai, T., Miyoshi, T., Nakano, S., Somekawa, H. and Higashi, K., 2006, Compressive response of a closed-cell aluminum foam at high strain rate. *Scripta Materialia*. 54(4): p. 533-537.

Odacı, İsmet Kutlay, 2011, The projectile impact responses of the composite faced aluminum foam and corrugated aluminum sandwich structures: A comparative study, İZTECH.

Paul, A. and Ramamurty, U., 2000, Strain rate sensitivity of a closed-cell aluminum foam. *Materials Science and Engineering A*. 281(1-2): p. 1-7.

Peroni, Lorenzo, Avalle, Massimiliano and Peroni, Marco, 2008, The mechanical behaviour of aluminium foam structures in different loading conditions. *International Journal of Impact Engineering*. 35(7): p. 644-658.

Reid, S. R. and Peng, C., 1997, Dynamic uniaxial crushing of wood. *International Journal of Impact Engineering*. 19(5-6): p. 531-570.

Ruan, D., Lu, G., Wang, B. and Yu, T. X., 2003, In-plane dynamic crushing of honeycombs--a finite element study. *International Journal of Impact Engineering*. 28(2): p. 161-182.

Shen, Jianhu, Lu, Guoxing and Ruan, Dong, 2010, Compressive behaviour of closed-cell aluminium foams at high strain rates. *Composites Part B: Engineering*. 41(8): p. 678-685.

Smerd, R., Winkler, S., Salisbury, C., Worswick, M., Lloyd, D. and Finn, M., 2005, High strain rate tensile testing of automotive aluminum alloy sheet. *International Journal of Impact Engineering*. 32(1-4): p. 541-560.

Tagarielli, V. L., Deshpande, V. S. and Fleck, N. A., 2008, The high strain rate response of PVC foams and end-grain balsa wood. *Composites Part B: Engineering*. 39(1): p. 83-91.

Tam, L. L. and Calladine, C. R., 1991, Inertia and strain-rate effects in a simple plate-structure under impact loading. *International Journal of Impact Engineering*. 11(3): p. 349-377.

Vural, M. and Ravichandran, G., 2003, Dynamic response and energy dissipation characteristics of balsa wood: experiment and analysis. *International Journal of Solids and Structures*. 40(9): p. 2147-2170.

Wierzbicki, Tomasz, 1983, Crushing analysis of metal honeycombs. *International Journal of Impact Engineering*. 1(2): p. 157-174.

Wu, Enboa and Jiang, Wu-Shung, 1997, Axial crush of metallic honeycombs. *International Journal of Impact Engineering*. 19(5-6): p. 439-456.

Zhao, H., Elnasri, I. and Abdennadher, S., 2005, An experimental study on the behaviour under impact loading of metallic cellular materials. *International Journal of Mechanical Sciences*. 47(4-5): p. 757-774.

Zhao, H., Elnasri, I. and Li, H. J., 2006, The Mechanism of Strength Enhancement under Impact Loading of Cellular Materials. *Advanced Engineering Materials*. 8(9): p. 877-883.

Zhao, Han and Abdennadher, Salim, 2004, On the strength enhancement under impact loading of square tubes made from rate insensitive metals. *International Journal of Solids and Structures*. 41(24-25): p. 6677-6697.

Zhao, Han and Gary, Grrard, 1998, CRUSHING BEHAVIOUR OF ALUMINIUM HONEYCOMBS UNDER IMPACT LOADING. *International Journal of Impact Engineering*. 21(10): p. 827-836.

Zheng, Zhijun, Yu, Jilin and Li, Jianrong, 2005, Dynamic crushing of 2D cellular structures: A finite element study. *International Journal of Impact Engineering*. 32(1-4): p. 650-664.